



1 **Formation and impacts of nitryl chloride in Pearl River Delta**

2 *Haichao Wang^{1,4}, Bin Yuan^{2,3,*}, E Zheng^{2,3}, Xiaoxiao Zhang^{2,3}, Jie Wang¹, Keding Lu^{5,6}, Chenshuo Ye^{2,3},*
3 *Lei Yang^{2,3}, Shan Huang^{2,3}, Weiwei Hu⁷, Suxia Yang^{2,3}, Yuwen Peng^{2,3}, Jipeng Qi^{2,3}, Sihang Wang^{2,3},*
4 *Xianjun He^{2,3}, Yubin Chen^{2,3}, Tiange Li^{2,3}, Wenjie Wang^{2,8}, Yibo Huangfu^{2,3}, Xiaobing Li^{2,3}, Mingfu*
5 *Cai^{2,3}, Xuemei Wang^{2,3}, Min Shao^{2,3}*

6 ¹ *School of Atmospheric Sciences, Sun Yat-sen University, Zhuhai, 519082, China*

7 ² *Institute for Environmental and Climate Research, Jinan University, Guangzhou 511443, China*

8 ³ *Guangdong–Hong Kong–Macau Joint Laboratory of Collaborative Innovation for Environmental*
9 *Quality, Guangzhou, 511443, China*

10 ⁴ *Guangdong Provincial Observation and Research Station for Climate Environment and Air Quality*
11 *Change in the Pearl River Estuary, Key Laboratory of Tropical Atmosphere-Ocean System, Ministry*
12 *of Education, Southern Marine Science and Engineering Guangdong Laboratory (Zhuhai), Zhuhai,*
13 *519082, China*

14 ⁵ *State Key Joint Laboratory of Environmental Simulation and Pollution Control, College of*
15 *Environmental Sciences and Engineering, Peking University, Beijing, 100871, China.*

16 ⁶ *The State Environmental Protection Key Laboratory of Atmospheric Ozone Pollution Control,*
17 *College of Environmental Sciences and Engineering, Peking University, Beijing, 100871, China*

18 ⁷ *State Key Laboratory of Organic Geochemistry and Guangdong Key Laboratory of Environmental*
19 *Protection and Resources Utilization, Guangzhou Institute of Geochemistry, Chinese Academy of*
20 *Sciences, Guangzhou 510640, China*

21 ⁸ *Multiphase Chemistry Department, Max Planck Institute for Chemistry, Mainz 55128, Germany*

22 *Correspondence: Bin Yuan (byuan@jnu.edu.cn)*



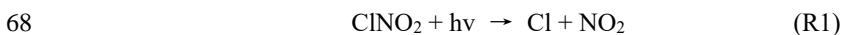
23 **Abstract.** Here we present a field measurement of ClNO₂ (nitryl chloride) and N₂O₅ (dinitrogen
24 pentoxide) by a Time-of-Flight Chemical Ionization Mass Spectrometer (ToF-CIMS) with the Filter
25 Inlet for Gas and AEROsols (FIGAERO) at a regional site in Pearl River Delta during a photochemical
26 pollution season from Sept. 26th to Nov. 17th, 2019. Three patterns of air masses are sampled during
27 this campaign, including the dominating air masses from north and northeast urban regions (Type A),
28 the southeast coast (Type B) and the South China Sea (Type C). The concentration of ClNO₂ and N₂O₅
29 were observed much higher in Type A and B than those in Type C, indicated the urban nighttime
30 chemistry is more active than the background marine regions. N₂O₅ uptake coefficient and ClNO₂
31 production yield were estimated by measured parameters, and the performance of the previously
32 derived parameterizations were assessed. The nighttime ClNO₂ correlated with particulate chloride
33 and the mass concentration of fine particles (most likely due to aerosol surface area), but not with
34 nitrate radical formation rate, suggested the ClNO₂ formation was limited by the N₂O₅ uptake rather
35 than N₂O₅ source at this site. By examining the relationship of particulate chloride and other species,
36 we implied that anthropogenic emissions (e.g., biomass burning) rather than sea salt particles dominate
37 the origin of particulate chloride, despite the site is only about 100 km away from the ocean. A box
38 model with detailed chloride chemistry is used to investigate the impacts of ClNO₂ chemistry on
39 atmospheric oxidation. Model simulations showed the chloride radical liberated by ClNO₂ photolysis
40 during the next day had a small increase in concentrations of OH, HO₂ and RO₂ radicals, as well as
41 minor contributions to RO₂ radical and O₃ formation (<5%, on daytime average) in all the three types
42 of air masses. Relative higher contributions were observed in Type A and B. The overall low
43 contributions of ClNO₂ to atmospheric oxidation are consistent with those reported recently from
44 wintertime observations in China (included Shanghai, Beijing, Wangdu and Mt. Tai). This may be
45 attributed to: (1) Relative low particle mass concentration limited ClNO₂ formation; (2) Other reactions
46 channels, like nitrous acid (HONO), oxygenated volatile organic compounds (OVOCs, including
47 formaldehyde) and ozone photolysis, had larger radical formation rate during the ozone pollution
48 episodes and weakened the ClNO₂ contribution indirectly. The results provided scientific insights into
49 the role of nighttime chemistry in photochemical pollution under various scenarios in coastal areas.
50



51 **1. Introduction**

52 Chloride radical is an important oxidant in the tropospheric besides OH radicals, NO₃ radicals and
53 ozone (Saiz-Lopez and von Glasow, 2012; Simpson et al., 2015; Wang et al., 2019b), which alters the
54 fate of many atmospheric compositions including oxidants, reactive nitrogen compounds, volatile
55 organic compounds (VOCs), and other halogens. Cl radical is much more reactive than OH with
56 respect to certain VOCs (e.g., alkanes) by a few orders of magnitude for reaction rate constant
57 (Atkinson and Arey, 2003; Atkinson et al., 2006), therefore, it contributes to atmospheric oxidation
58 capacity considerably in the troposphere despite low concentrations. For example, global model
59 showed about 20 % of ethane, 14 % of propane oxidation are attributed to the chloride chemistry at
60 the global scale (Wang et al., 2019c). Modeling simulations also demonstrated chloride chemistry
61 enhanced oxidative degradation of VOCs by >20% at some locations (Sarwar et al., 2014).

62 Photolysis of ClNO₂ (R1) is a major source of the tropospheric chloride radical (Thornton et al.,
63 2010b; Simpson et al., 2015), other chloride radical sources include the reaction of HCl with OH
64 (Riedel et al., 2012; Eger et al., 2019), photolysis of Cl₂ and other halogen compounds like ICl and
65 BrCl (Peng et al., 2021). Tropospheric ClNO₂ is not only an important chlorine activation precursor
66 but also a nocturnal reservoir of reactive nitrogen, which is mainly formed in heterogeneous reaction
67 of N₂O₅ on chlorine-containing particles with a branch ratio at nighttime (R2).



70 where φ represents the yield of ClNO₂. This mechanism was firstly proposed by Finlaysonpitts et al.
71 (1989) through detecting the products of N₂O₅ uptake on NaCl particles. Given this reaction, the
72 formation of ClNO₂ can be influenced by the N₂O₅ uptake (such as N₂O₅ uptake probabilities and
73 aerosol surface area) as well as the production yield of ClNO₂.

74 N₂O₅ uptake coefficient, $\gamma(\text{N}_2\text{O}_5)$, have been reported highly varied under tropospheric conditions
75 (Brown and Stutz, 2012). Both the field and laboratory studies revealed that this process can be affected
76 by ambient temperature, relative humidity (Mozurkewich and Calvert, 1988; Mentel et al.,
77 1999; Hallquist et al., 2003), chemical compositions (such as the content of nitrate, liquid water,
78 chloride, and organics) (Mentel et al., 1999; Brown et al., 2006; Bertram and Thornton, 2009; Gaston et
79 al., 2014; McDuffie et al., 2018b; Tang et al., 2014; Anttila et al., 2006), as well as particle morphology
80 (Mielke et al., 2013; Zong et al., 2021). Until now, the key factors that controlling N₂O₅ uptake



81 coefficient in the different environments are still not well understood. ClNO₂ yield is also highly varied
82 subject to the liquid water and chloride content in the aerosol (Behnke et al., 1997;Roberts et al.,
83 2009;Bertram and Thornton, 2009). Several studies demonstrated that the ClNO₂ yield is also affected
84 by other factors like aerosol sulfate (Staudt et al., 2019) and organics (Ryder et al., 2015;Tham et al.,
85 2018;McDuffie et al., 2018a). However, the comprehensive quantitative relationship of these factors
86 in controlling the yield still has large uncertainties. These gaps in understanding the critical controlling
87 factors for N₂O₅ uptake coefficient as well as ClNO₂ yield lead to the prediction of ClNO₂ and
88 particulate nitrate production very challenge.

89 Osthoff et al. (2008) and Thornton et al. (2010a) directly observed elevated ClNO₂ in coastal and
90 inland U.S. by chemical ionization mass spectrometer (CIMS), respectively. They shed light on the
91 significance of ClNO₂ photolysis in launching the radical chemistry during the morning time, and also
92 affecting halogen chemistry and reactive nitrogen cycling. Large amounts of chloride radicals are
93 liberated through the photolysis of nocturnal accumulated ClNO₂ (R1), which oxidizes VOCs and
94 produces peroxy radicals (RO₂) to initiate the daytime radical cycling in the morning, when other
95 radical source, like ozonolysis and photolysis of O₃, HONO and HCHO, are still weak (Osthoff et al.,
96 2008). The impacts of ClNO₂ chemistry on primary source of radicals and ozone formation is a critical
97 topic, the answer of which is very helpful to narrow the gap of the missing primary source of RO_x and
98 improve our knowledge of the current ozone pollution mechanism (Tan et al., 2017;Tham et al., 2016).
99 Model simulation highlighted ClNO₂ chemistry could increase mean daily maximum 8 h ozone by up
100 to 7.0 ppbv in some areas in the Northern Hemisphere (Sarwar et al., 2014). The large contribution
101 was also confirmed in the southern California region by a box model study (Riedel et al., 2014). In
102 addition, global model simulation showed ClNO₂ chemistry increases wintertime ozone by up to 8 ppb
103 over polluted continents (Wang et al., 2019c). Particularly, previously modelling results also highlight
104 the importance of ClNO₂ chemistry in enhancing O₃ production in China (Li et al., 2016;Yang et al.,
105 2022b).

106 Several field studies reported the measurement of ClNO₂ in varied environments in the past decade
107 (Riedel et al., 2012;Young et al., 2012;Mielke et al., 2013;Riedel et al., 2013;Bannan et al., 2015;Faxon
108 et al., 2015;Mielke et al., 2015;Phillips et al., 2016;Bannan et al., 2017;Wang et al., 2017c;Wang et al.,
109 2017d;Le Breton et al., 2018;McDuffie et al., 2018a;Yun et al., 2018a;Zhou et al., 2018;Bannan et al.,
110 2019;Eger et al., 2019;Haskins et al., 2019;Jeong et al., 2019;Xia et al., 2020;Xia et al., 2021;Tham et
111 al., 2016;Tham et al., 2014;Wang et al., 2016;Phillips et al., 2012;Lou et al., 2022;Sommariva et al.,
112 2018), in which the maximum ClNO₂ up to sub-ppbv to several ppbv were reported, indicating its
113 ubiquity presence worldwide and a broad atmospheric impacts over various regions. During the
114 CalNex-LA campaign 2010, ClNO₂ was measured at ground site, the Research Vessel and aircraft



115 platform, which depicted a full picture of the abundance of ClNO₂ and confirmed its large impacts on
116 atmospheric chemistry in both urban and coastal regions in California (Riedel et al., 2012; Young et al.,
117 2012; Mielke et al., 2013). Recently, Wang et al. (2016) used a box model simulated the chemical
118 evolution of the plume after leaving the observation site in Hongkong and showed ClNO₂ chemistry
119 had a following-day enhancement of ozone peak and daytime ozone production rate by 5–16% and
120 11–41%, along with a large increasing of OH, HO₂ and RO₂ concentration especially in the morning.
121 While Xia et al. (2021) and Lou et al. (2022) reported winter measurements of ClNO₂ in north and east
122 China, respectively, both they showed moderate ClNO₂ level and a relative small contributions of
123 ClNO₂ chemistry to radical source and ozone enhancement on campaign average. These results is quite
124 different with that happened during the summertime in China (Tham et al., 2016; Wang et al., 2016; Tan
125 et al., 2017), and highlight the large variation of ClNO₂ chemistry influenced by temporal spatial
126 distribution.

127 Despite its likely importance to the regional atmospheric oxidation and air quality, investigations of
128 ClNO₂ chemistry in China remain relatively sparse. There are several field measurements of ClNO₂
129 conducted in the China in recent years, while considering the large diversities of air mass in inland and
130 coastal regions in China, more field and model works are need to gain more insights to the ClNO₂
131 chemistry in various atmospheric environments and assess its atmospheric impacts. Until now, only
132 several field measurement of ClNO₂ were reported in Pearl River Delta (PRD) region (Tham et al.,
133 2014; Wang et al., 2016; Yun et al., 2018a), and only Wang et al. (2016) reported a comprehensive
134 analysis of the impact of ClNO₂ chemistry on radical and ozone formation in 2013 as mentioned before.
135 To understanding the increasing O₃ problem in recent years (Wang et al., 2019a) and examining the
136 role of ClNO₂ chemistry in O₃ formation in PRD, we measured ClNO₂, N₂O₅, and other related
137 parameters at a regional site in PRD during a severe photochemical pollution season in 2019. The
138 abundance, formation, and variation during different air masses patterns are well characterized. The
139 factors impact its formation are diagnosed. Finally, the contribution of chloride radicals liberated by
140 ClNO₂ photolysis on the daytime radical chemistry, as well as ozone formation are comprehensively
141 assessed by a box model coupled with detailed chloride chemistry.

142 **2. Method**

143 **2.1 Measurement site**

144 This campaign was conducted at the Guangdong Atmospheric Supersite of China, which is located on
145 the top of a mountain (~ 60 m high) in Heshan (22.728°N, 112.929°E), Jiangmen city, Guangdong
146 Province (Yang et al., 2022a). This site was in the western Peral River Delta where no major industry
147 in the surroundings, but with some farmland and a few residents live at the hill foot. The traffic is far



148 away from this site and believed seldom disturbs the sampling. The anthropogenic activity is much
149 lower than the urban regions like Guangzhou City, but the air quality is often influenced by neighbor
150 cities, especially the outflow of air masses from the regions on the north and northeast. Therefore, the
151 air masses sampled at this site are representative of the urban pollution from the center PRD. There
152 were many atmospheric intensive studies once conducted in the site to study the air pollutions in PRD
153 (Tan et al., 2019; Yun et al., 2018b). In this study, the instruments were located on the top floor of the
154 measurement building with inlets approximately 15 m above the ground. The data presented in the
155 study were collected from 27th September to 17th November 2019, during which photochemical
156 pollution occurred frequently (Yang et al., 2022a). Time is given as CNST (Chinese National Standard
157 Time = UTC+8 h). During the campaign, sunrise was at 06:00 and sunset was at 18:00 CNST.

158 2.2 Instrument setup

159 A comprehensive suite of instrumentation was overviewed and listed in Table 1. An iodide-adduct
160 Time-of-Flight Chemical Ionization Mass Spectrometer (ToF-CIMS) with the Filter Inlet for Gas and
161 AEROSols (FIGAERO) was applied to measure ClNO₂ and N₂O₅ along with other oxygenated organic
162 species (Ye et al., 2021; Wang et al., 2020b). In brief, the gas phase species were measured via a 2-m-
163 long, 6-mm-outer-diameter PFA inlet while the particles were simultaneously collected on a Teflon
164 filter via a separate 2-m-long, 10-mm-outer-diameter copper tubing inlet; both had flow rates of 2 L
165 min⁻¹ with a drainage flow of 20 L min⁻¹. The gas phase was measured for 25 minutes at 1 Hz, and the
166 FIGAERO instrument was then switched to place the filter in front of the ion molecule region; it was
167 then heated incrementally to 200 °C to desorb all the mass from the filter to be measured in the gas
168 phase, which resulted in high-resolution thermograms. ClNO₂ and N₂O₅ are measured as the iodide
169 adduct ions at m/z 207.867 (IClNO₂⁻) and m/z 234.886 (IN₂O₅⁻) in the ToF-CIMS, respectively. The
170 sensitivities for detecting ClNO₂ and N₂O₅ with the dependence of water content were quantified and
171 described in details (see Appendix). The limit of detection (LOD) for ClNO₂ and N₂O₅ were 4.3 and
172 6.0 pptv in 1-minute time-resolution, respectively, with an uncertainty of ~30%.

173 Sub-micron aerosol composition (PM₁) were measured by a High-Resolution Time of Flight Aerosol
174 Mass Spectrometer (HR-ToF-AMS) (DeCarlo et al., 2006). The soluble ions of sodium and potassium
175 was measured by a commercial instrument (GAC-IC) equipped with an aerosol collector and detected
176 by ion chromatography (Dong et al., 2012). The particle number size distribution (PNSD) was
177 measured by a scanning mobility particle sizer (SMPS, TSI 3938). The aerosol surfaces area was
178 calculated based on the size distribution measurement and corrected to wet particle-state by a
179 hygroscopicity growth factor, with a total uncertainty of determining wet aerosol surface areas by ~30%
180 (Liu et al., 2013). VOCs were measured by Proton Transfer Reaction Time-of-Flight Mass



181 Spectrometry (PTR-MS)(Wu et al., 2020;He et al., 2022) and an automated gas chromatograph
182 equipped with mass spectrometry or flame ionization detectors (GC-MS). A commercial instrument
183 (Thermo Electron model 42i) was used to monitor NO_x. O₃ was measured by a commercial instrument
184 using ultraviolet (UV) absorption (Thermo Electron 49i). PM_{2.5} was measured by a Tapered Element
185 Oscillating Microbalance (TEOM, 1400A analyzer). SO₂ and CO were measured by commercial
186 instruments (Thermo Electron 43i and 48i). In addition, the meteorological parameters were available
187 during the measurement. Photolysis frequencies were determined by a spectroradiometer (Bohn et al.,
188 2008). The aerosol liquid water content (ALWC) is calculated from the ISORROPIA-II
189 thermodynamic equilibrium model (Clegg et al., 1998). We used the reverse mode in ISORROPIA-II
190 with the input of water-soluble ions along with ambient temperature (*T*) and relative humidity (RH).
191 Given the high RH in this campaign, we ran the model by assuming aerosol phase were metastable.

192 **Table 1.** Summary of the information about observed gas and particle parameters during the campaign.

Species	Limit of detection	Methods	Accuracy
N ₂ O ₅	6.0 pptv (3σ, 1 min)	FIGAERO-ToF-CIMS	± 30%
ClNO ₂	4.3 pptv (3σ, 1 min)	FIGAERO-ToF-CIMS	± 30%
NO	60 pptv (2σ, 1 min)	Chemiluminescence	± 20%
NO ₂	0.3 ppbv (2σ, 1 min)	Mo convert	± 20%
O ₃	0.5 ppbv (2σ, 1 min)	UV photometry	± 5%
VOCs	0.1 ppbv (5 min)	PTR-ToF-MS	± 30%
VOCs	20-300 pptv (1 h)	GC-FID/MS	± 20%
PM _{2.5}	0.1 μg m ⁻³ (1 min)	TEOM	± 5%
CO	4 ppbv (5 min)	IR photometry	± 5%
SO ₂	0.1 ppbv (1 min)	Pulsed UV fluorescence	± 10%
HCHO	25 pptv (2 min)	Hantzsch fluorimetry	± 5%
PNSD	14 nm -700 nm (4 min)	SMPS	± 20%
Aerosol composition	<0.16 μg m ⁻³ (30 min)	GAC-IC	± 30%
PM ₁ components	0.15 μg m ⁻³ (4 min)	HR-ToF-AMS	± 30%
Photolysis frequencies	Varies with species (20 s)	Spectroradiometer	± 10%

193

194 **2.3 Box model setup**

195 A zero-dimensional chemical box model constrained by the field campaign data was applied to
196 simulate the ClNO₂ chemistry. The box model was based on the Regional Atmospheric Chemical
197 Mechanism version 2 (RACM2) described in Goliff et al. (2013), and chloride chemical mechanism
198 were added (Wang et al., 2017b;Tan et al., 2017). Briefly, chloride chemistry was adapted to RACM2
199 from the modifications to Master Chemical Mechanism (Xue et al., 2015), and the oxidation products
200 from reactions between lumped VOC species and chloride radicals were adapted from those of OH

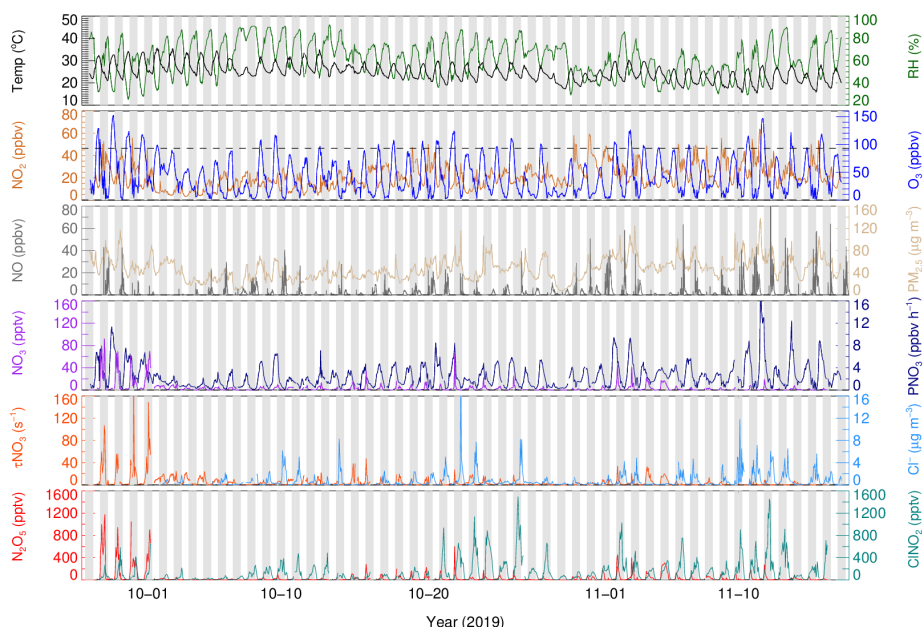


201 oxidation from RACM2.j(CINO₂) was calculated according to the NASA-JPL recommendation based
202 on the work by Ghosh et al. (2012). The impact of O₃ by CINO₂ chemistry was assessed by differing
203 the results of two scenarios with or without the constraints of the observed CINO₂ in the model
204 simulation. For the reaction rate constant of the lumped species with Cl, the fastest value from different
205 species was used to represent the upper limit of the impact of chloride chemistry. The model was
206 constrained by the observed CINO₂, NO_x, O₃, CO, VOCs (assignment to RACM2), photolysis
207 frequencies, ambient temperature and pressure. The model runs were from 29 September to 17
208 November, 2019 with most of the measurement data taken accounted for, and with a two-days spin-
209 up. The lifetime of the input trace gases corresponds to a deposition velocity of 1.2 cm s⁻¹ with an
210 assumed boundary layer height of 1000 m, and the model-generated species was set to 24 hours
211 lifetime due to the loss caused by the dry deposition. The input data were averaged and interpolated to
212 1 hour of resolution.

213 3. Results and discussions

214 3.1 Overview of measurement

215 Figure 1 shows time series of CINO₂ and relevant trace gases, particles and meteorological parameters
216 during the measurements. In this campaign, the meteorological condition featured high temperature
217 (24.7 ± 3.8 °C) and high humidity ($62.1\% \pm 15.6\%$), low wind speed (1.5 ± 0.8 m s⁻¹), and the dominant
218 air flow were from north and northwest. Compared to those with previously measurements at the same
219 site in January 2017 (Yun et al., 2018b), the temperature was higher and relative humidity was lower
220 during the measurements. The average and maximum concentration of particulate matter (PM_{2.5}) was
221 47.6 ± 19.3 µg m⁻³ and 138 µg m⁻³, respectively, which is significantly lower than that observed in
222 January 2017, with a maximum up to 400 µg m⁻³. The dominant air pollutant was O₃ with hourly
223 campaign maximum and the average mean daily maximum 8-hour O₃ (MDA8 O₃) of 152.8 ppbv and
224 75.2 ± 20.9 ppbv, respectively. There were 27 days out of 53 days with the hourly maximum of O₃
225 exceeded the Chinese national air quality standard (200 µg m⁻³, equivalent to 93 ppbv), suggesting
226 severe ozone pollution during the measurement period in PRD region. NO₂ concentration was also
227 elevated with 21.0 ± 10.4 ppbv on campaign average. The concurrent high O₃ and NO₂ made large
228 nitrate radical production rate occurred with a daily average of 1.8 ± 2.1 ppbv h⁻¹. The campaign
229 maximum NO₃ production rate was observed up to 18.6 ppbv h⁻¹ in the afternoon at 11th November,
230 2019. However, high NO₃ production rate did not mean high concentrations of NO₃, N₂O₅ and CINO₂
231 in the atmosphere, as the concentration affected by both their sources and sinks.



232

233 **Figure 1.** Time series of N_2O_5 , ClNO_2 and relevant parameters. The grey dotted line in the O_3 panel
234 denotes Chinese national air quality standard for hourly maximum O_3 ($200 \mu\text{g m}^{-3}$, equivalent to 93
235 ppbv). NO_3 radical is calculated based on a thermal equilibrium with measured NO_2 and N_2O_5 .

236 N_2O_5 existed at a moderate concentration at most nights, with the daily nocturnal peaks range from
237 <100 pptv to 1180 pptv and nocturnal average of 64 ± 145 pptv. During the nights from 27th – 30th
238 September, 2019, the N_2O_5 concentration was significantly higher than other nights. The NO_3 lifetime,
239 calculated by steady state method (Brown et al., 2003), was much longer in the four nights than other
240 nights, implied relative weak sink of NO_3 - N_2O_5 for the first four nights. The lifetime of NO_3 was < 1
241 minute in general (except the first four nights), indicating active NO_3 chemistry at this site. The NO_3
242 concentration was calculated assuming the thermal equilibrium of NO_2 - NO_3 - N_2O_5 , with a possible
243 lower bias caused by the equilibrium coefficient for reversible reactions of NO_3 and N_2O_5 (K_{eq}) (Chen
244 et al., 2022). Figure 1 shows the variation of calculated NO_3 coincided with N_2O_5 . Elevated NO_3
245 occurred at the first four nights with a maximum of 90 pptv (1 h time resolution), which is comparable
246 with the reported NO_3 level at other sites in Pearl River Delta (Wang and Lu, 2019; Brown et al., 2016).
247 ClNO_2 showed a clear diurnal variation with high level during the night. The nocturnal average and
248 hourly maximum were 198 ± 232 pptv and 1497 pptv, respectively. The abundance of ClNO_2 and N_2O_5
249 are lower than those observed at the same site in 2017, with high N_2O_5 and the highest value ever
250 observed ClNO_2 of 3358 pptv and 8324 pptv (1-minute time resolution), respectively (Yun et al.,



251 2018b). High particulate chloride ion was observed in the site with $0.74 \pm 1.33 \mu\text{g m}^{-3}$ on nocturnal
252 average, which was higher at night with a peak in the second half of night and decrease at daytime.

253 3. 2 Characterization of pollutants in different air masses.

254 We noticed the air mass is highly varied during the measurements. For example, during the period of
255 10/02 - 10/05, the observed ozone and ClNO_2 were much lower than other days; while during the
256 period of 11/11 - 11/13, the air masses were much polluted with high O_3 , $\text{PM}_{2.5}$ and ClNO_2 . We
257 therefore plotted the backward trajectories of 24 h history of air masses arriving at the measurement
258 site at 500 m height at 00:00, 06:00, 12:00, 18:00 day by day. The measurement period was separated
259 into three patterns meteorologically according to the analysis of backward trajectories. Table 2 listed
260 the detailed information about the air mass classification. The air masses from northeast (and north)
261 was the dominant with a total of 37 days, which was characterized with the outflow of the center city
262 clusters of PRD and those from inland through long distance transport. We checked the pollutants of
263 the air masses from PRD and the north out of PRD (e.g., Hunan or Jiangxi Province), while no
264 significant difference was found. Therefore, we merged the two inland air masses as Type A. The
265 second type was from the coastal or offshore from east and southeast (Type B), which features the
266 outflow of coastal cities like Shenzhen and Hong Kong, which occurred on 12 days in total. The third
267 type was the clean air masses from the South China Sea (4 days, Type C). Figure 2 shows three cases
268 of each air masses mentioned above.

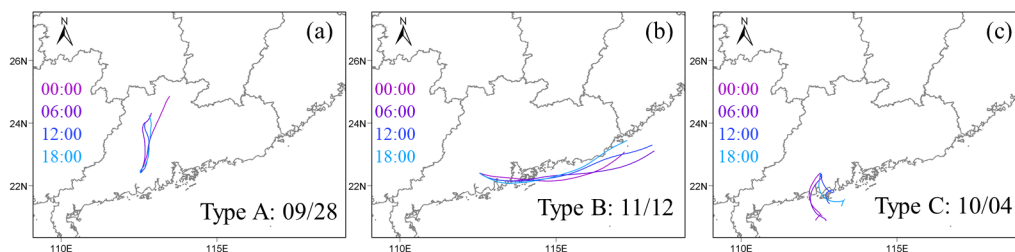
269 **Table 2.** The detailed information of three air mass types.

Air mass type	Periods	Days
Type A: inland air from northeast	09/26-10/01;10/08;10/11-10/20;10/24- 11/10;11/14-15	37 (69.8%)
Type B: coast air from east	10/06-07; 10/09-10; 10/21-23; 11/11-13; 11/16-17	12 (22.6%)
Type C: marine air from south	10/02-05	4 (7.5%)

270 The mean diurnal profiles of measured NO_2 , O_3 , N_2O_5 , ClNO_2 , the particle chloride content and the
271 ratio of chloride to sodium in the three types of air masses are shown in Figure 3, with a detailed
272 summary of related parameters in nocturnal medians listed in Table 3. High levels of NO_2 and O_3 were
273 observed in Type A and B air masses, with small difference of NO_2 diurnal variation during the second
274 half of night. In comparison, the two pollutants in Type C were much lower. If we focus on the
275 abundance at night, we found a large difference in NO_2 level with a sequence Type A > Type B > Type
276 C, which results in the same sequence of NO_3 productions in different air masses. The nocturnal NO_2
277 seems to be a good indicator of the level of pollution, that nocturnal CO, $\text{PM}_{2.5}$ and SO_2 also followed

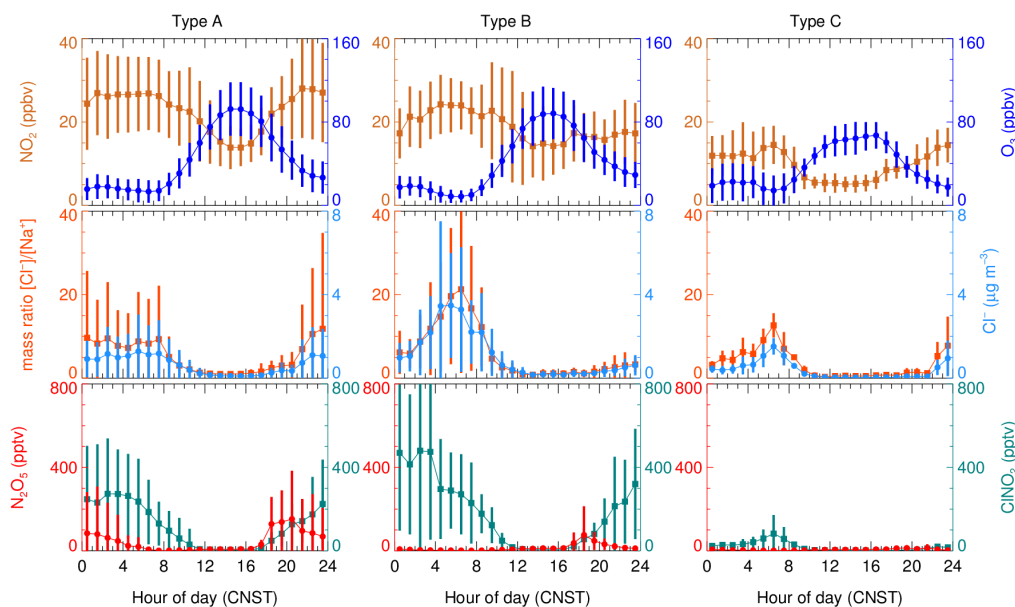


278 this order with highest concentration in Type A. These results indicate that the most polluted air mass
279 came from the inland urban regions of PRD.



280
281 **Figure 2.** Three typical cases with air mass from different regions at 29th Sept., 12th Nov. and 4th Oct.,
282 respectively. Backward trajectory of 24 h history of air masses arriving at the measurement site with
283 500 m height at 00:00, 06:00, 12:00, 18:00.

284 Given the particulate chloride a precursor of ClNO₂, we examined its diurnal variations in the three
285 air mass types. The highest level of Cl⁻ was found in Type B, and then followed by Type A and Type
286 C (also at night). Although the diurnal profile of Cl⁻ in the three types is similar, the increasing rate of
287 Cl⁻ during the second half of night in Type A is much slower than those in coastal and offshore air
288 masses. This imply a difference source of chloride, which will be further discussed in the Section 3.4.
289 N₂O₅ was observed with moderate concentration in the Type A air mass throughout the night, with a
290 nocturnal peak of 152.4 pptv between 20:00-21:00, while little N₂O₅ only occurred in the first half of
291 night in Type B and C with a peak of 75.9 pptv and 13.6 pptv, respectively. The concentration
292 difference may be attribute to two aspects. Firstly, the difference of P(NO₃) results in more N₂O₅
293 produced in Type A. Secondly, compared with the air mass from coastal or offshore regions, the
294 nocturnal temperature and RH condition from Type A is much lower, and the loss of N₂O₅ may be
295 faster in Type B and C than that in Type A. The nocturnal median RH in Type A reached up to 67%,
296 while 78% and 79% in Type B and Type C, suggesting a favorable condition for heterogeneous
297 hydrolysis of N₂O₅ for all the three air mass types. The elevated ClNO₂ was observed in Type A and B
298 with a nocturnal peak of 273.6 pptv and 479.8 pptv, respectively. Significantly less ClNO₂ was
299 observed in Type C air mass with a peak of 82.6 pptv. The reason of the different levels of ClNO₂
300 observed in the three air masses types are discussed in Section. 3.4.



301

302 **Figure 3.** Mean diurnal profiles of N_2O_5 , ClNO_2 and relevant parameters in the three types of air
 303 masses.

304 **Table 3.** Statistics results (median \pm standard deviation) of the related parameters in the three types
 305 of air masses (from 18:00 to 06:00 CNST).

Air mass	Type-A	Type-B	Type-C
RH (%)	67.0 ± 11.9	78.0 ± 10.9	79.0 ± 9.1
T (°C)	22.8 ± 3.0	23.3 ± 2.2	25.6 ± 1.9
ClNO_2 (pptv)	131.0 ± 202.8	162.0 ± 310.1	16.7 ± 21.2
N_2O_5 (pptv)	17.8 ± 164.9	6.3 ± 64.6	2.8 ± 9.3
Cl^- ($\mu\text{g m}^{-3}$)	0.41 ± 1.11	0.56 ± 1.85	0.33 ± 0.51
$\text{PM}_{2.5}$ ($\mu\text{g m}^{-3}$)	53.0 ± 18.8	41.0 ± 21.8	32.0 ± 10.2
SO_2 (ppbv)	5.0 ± 4.7	3.4 ± 11.4	3.4 ± 4.7
Na^+ ($\mu\text{g m}^{-3}$)	0.12 ± 0.07	0.18 ± 0.09	0.09 ± 0.03
$\text{P}(\text{NO}_3)$ (ppbv h^{-1})	1.60 ± 1.49	1.39 ± 1.50	0.69 ± 0.49
NO_2 (ppbv)	24.8 ± 10.9	18.1 ± 6.2	11.2 ± 5.8
O_3 (ppbv)	24.4 ± 21.8	29.5 ± 23.1	22.4 ± 15.2
CO (ppbv)	540.3 ± 122.3	448.4 ± 130.7	367.5 ± 89.8

306 3.3 N_2O_5 uptake coefficient and ClNO_2 yield

307 In line with previous studies, we estimate N_2O_5 uptake coefficient and ClNO_2 yield using the
 308 measurements of N_2O_5 , ClNO_2 and particulate nitrate (Phillips et al., 2016; Wang et al., 2018; Tham et
 309 al., 2018). By assuming both the nocturnal enhancement of nitrate and ClNO_2 are mainly attributed to



310 N_2O_5 uptake processes, ClNO_2 yield can be solely derived by the regression analysis of ClNO_2 versus
311 particulate nitrate (Wagner et al., 2012; Riedel et al., 2013). The ϕClNO_2 can then be obtained by the
312 fitted regression slope (S, Eq. 1) and named as regression method.

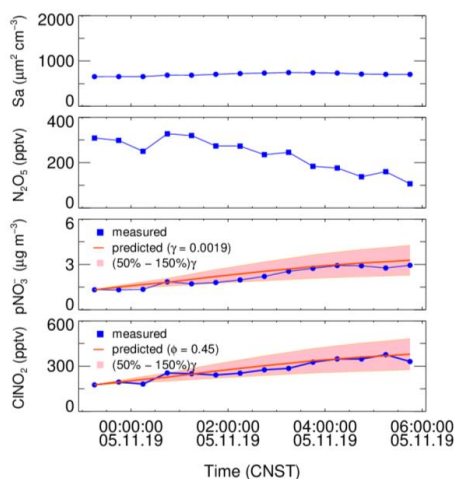
$$313 \quad \phi = 2S/(S+1) \quad (\text{Eq. 1})$$

314 Combining with the data of N_2O_5 and aerosol surface area, the increase in ClNO_2 and nitrate can
315 be simulated simultaneously by setting the input of N_2O_5 uptake coefficient and ClNO_2 yield (named
316 as simulation method). The optimal N_2O_5 uptake coefficient and ClNO_2 yield are obtained
317 simultaneously by adjusting the two parameters until the simulation reproduces the observed increase
318 ClNO_2 and nitrate (Phillips et al., 2016; Xia et al., 2020; Tham et al., 2018). This analysis assumes only
319 N_2O_5 uptake process dominates the increase of ClNO_2 and nitrate, and other physicochemical
320 processes like vertical transportation, depositions are less important. This method requests the air mass
321 in the analysis duration time is relative stable and less affected by emission and transportation. In
322 addition, it is not valid in the case with negative changes of ClNO_2 and nitrate. The following selection
323 criteria is set to pick out the suitable plumes to meet the assumptions. Firstly, the consistent increase
324 trends of ClNO_2 and the NO_3^- and clear correlation between them during the analysis duration should
325 be observed with a regression coefficient threshold of 0.5, which indicates the two products have the
326 same source. Secondary, an equivalent or faster increase of ammonium accompanied with nitrate, to
327 ensure insignificant degas of HNO_3 to the atmosphere. The observational data were averaged to 30
328 min for the following analysis, the time-period of each derivation ranges from 2.5 to 10 hours. Figure
329 4 depicts an example of the derivation on 5th November, 2019, the stable Sa indicates stable air mass
330 during the analysis period. And the prediction is well reproduced the observed increase in ClNO_2 and
331 NO_3^- .

332 During this campaign, we carefully identified 20 plumes with clear correlations between ClNO_2
333 and particulate nitrate by the slope method ($R^2 \geq 0.5$). As shown in Table 4, the derived ClNO_2 yield
334 varied from 0.13 to 1.00 with a median of 0.45 ± 0.22 (mean value of 0.44). In the 20 plumes, we
335 derived N_2O_5 uptake coefficient and ClNO_2 for 12 cases in total. The results in other 8 night were not
336 valid due to the lack of Sa data (four nights) or producing unreasonably high results due to the observed
337 low N_2O_5 concentration near the detection limit biased the simulations. We show good consistent of
338 derived ClNO_2 yields by the two different methods. The estimated N_2O_5 uptake coefficient showed a
339 large variation and ranged from 0.0019 to 0.077 with a median of 0.0195 ± 0.0288 (mean value of
340 0.0317). The estimated $\gamma\text{N}_2\text{O}_5$ is within the range determined by previous field studies (Tham et al.,
341 2018). Specifically in China, the average level of $\gamma\text{N}_2\text{O}_5$ is comparable with those reported in urban
342 Beijing (Wang et al., 2017a; Wang et al., 2018), Wangdu (Tham et al., 2018), and Jinan (Wang et al.,
343 2017c) during the summertime, but systematically higher than those determined in China in wintertime



344 (Xia et al., 2021; Wang et al., 2020a; Brown et al., 2016), except the case reported on the urban canopy
 345 of Beijing (Chen et al., 2020). McDuffie et al. (2018a) summarized the reported ϕClNO_2 based on the
 346 observations, and we showed that the estimated average ϕClNO_2 in this study is in the middle to upper
 347 end of the values reported globally (Xia et al., 2021; McDuffie et al., 2018a). Due to the limited data
 348 points, we cannot distinguish the difference of $\gamma\text{N}_2\text{O}_5$ between the three air mass patterns. The ClNO_2
 349 yields in Type A are slightly lower than those in Type B with an average of 0.41 and 0.47, respectively.



350
 351 **Figure 4.** An example of the derivation of N_2O_5 uptake coefficient and ClNO_2 yield constrained by
 352 observation of aerosol surface area, N_2O_5 and the enhancement of particulate nitrate and ClNO_2 on 5th
 353 November, 2019. The pink region presents $\pm 50\%$ uncertainty of N_2O_5 uptake coefficient.

354 **Table 4.** The derived N_2O_5 uptake coefficient and ClNO_2 yields at each night.

NO.	Period	$\gamma\text{N}_2\text{O}_5^a$	ϕClNO_2^a	ϕClNO_2^b	r^{2b}	Type
1	10/02 01:00-06:00	NaN	NaN	0.13	0.90	C
2	10/02 23:00-06:00	NaN	NaN	0.25	0.90	C
3	10/11 01:00-04:00	NaN	NaN	0.65	1.00	B
4	10/14 23:00-04:00	0.017	0.28	0.23	0.56	A
5	10/18 18:00-21:00	0.0059	0.42	0.40	0.90	A
6	10/20 20:30-23:00	0.045	0.44	0.47	0.71	A
7	10/21 20:30-01:00	0.061	0.52	0.54	0.90	B
8	10/22 22:30-05:00	0.066	0.58	0.61	0.62	B
9	10/24 22:00-06:00	0.065	0.26	0.23	0.74	A
10	10/25 21:00-02:00	0.077	1.00	1.00	0.92	A
11	10/28 21:00-04:00	NaN	NaN	0.15	0.74	A
12	11/01 21:00-23:30	0.022	0.35	0.32	0.83	A
13	11/02 22:00-00:30	NaN	NaN	0.29	1.00	A



14	11/03 18:00-06:00	0.0031	0.52	0.50	0.92	A
15	11/04 22:00-06:00	0.0019	0.45	0.47	0.86	A
16	11/08 00:00-06:00	0.0097	0.34	0.32	0.85	A
17	11/10 00:00-04:00	NaN	NaN	0.59	0.80	A
18	11/11 22:00-04:00	NaN	NaN	0.53	0.50	B
19	11/12 22:00-04:00	NaN	NaN	0.42	0.62	B
20	11/13 21:00-00:00	0.0070	0.70	0.75	0.92	B

355 Note: ^a the values of $\gamma\text{N}_2\text{O}_5$ and ϕClNO_2 are derived by simulation method; ^b the ϕClNO_2 and the
356 correlation coefficient (R^2) between ClNO_2 and particulate nitrate are derived by regression method,
357 the data was filtered with a correlation coefficient obtained from linear fitting threshold of 0.5.

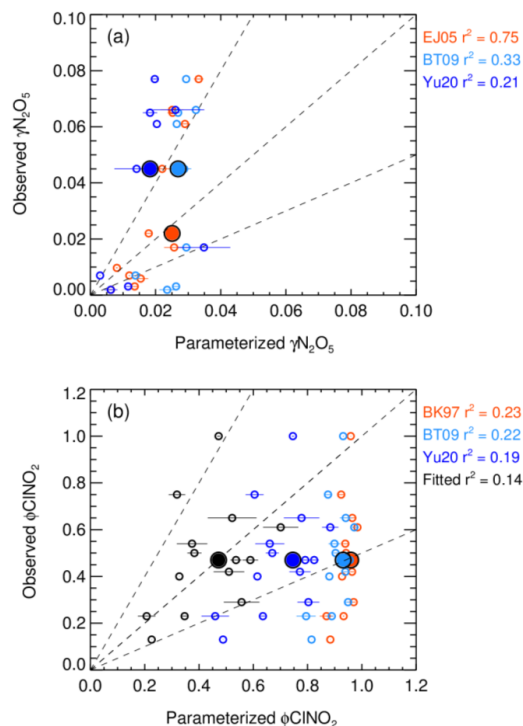
358 To gain insight into the factors governing the N_2O_5 uptake and ClNO_2 formation processes, the
359 estimated $\gamma\text{N}_2\text{O}_5$ and ϕClNO_2 were compared with those predicted from complex laboratory-derived
360 and field-derived parameterizations. An aqueous inorganic ionic reaction mechanism once raised by
361 Bertram and Thornton (2009) and established a volume-limited parameterization by considering the
362 aerosol volume, surface area, nitrate content, ALWC, and chloride content (named BT09, Eq. 8).

$$363 \gamma_{BT09} = \frac{4H_{aq}Vk}{CS_a} \left(1 - \frac{1}{1 + \frac{k_3[\text{H}_2\text{O}]}{k_{2b}[\text{NO}_3^-]} + \frac{k_4[\text{Cl}^-]}{k_{2b}[\text{NO}_3^-]}} \right) \quad (8)$$

364 Where H_{aq} is Henry's law coefficient of N_2O_5 , V is the aerosol volume; k is equal to $1.15 \times 10^6 - (1.15$
365 $\times 10^6)^{\exp(-0.13[\text{H}_2\text{O}])}$; k_3/k_{2b} is the ratio of reaction rate of H_2O versus NO_3^- to H_2ONO_2^+ that was set to
366 0.06, and k_4/k_{2b} is the ratio of reaction rate of Cl^- versus NO_3^- to H_2ONO_2^+ that was set to 29 (Bertram
367 and Thornton, 2009). The mean values of particulate volume to surface ratio (V/S_a) was measured. A
368 simple parameterization (EJ05) considered the effect of enhanced RH and temperature on N_2O_5 uptake
369 was also included (Evans and Jacob, 2005). In addition, the recently established empirical
370 parameterization based on the same framework (Eq. 8, named Yu20), optimized some parameters
371 according to the meta-analysis of five field measurements in China by Yu et al. (2020), also assessed
372 in the study. Figure 5(a) shows the correlation of estimated $\gamma\text{N}_2\text{O}_5$ versus the parameterization. All the
373 three parameterizations fail to predict the high values. The simple parameterization of EJ05 had the
374 best performance with a high correlation and a consistent prediction of the median value. While other
375 two parameterizations, BT09 and Yu20, underestimated the observed $\gamma\text{N}_2\text{O}_5$. Figure 6(a-h) show the
376 dependence of the observed $\gamma\text{N}_2\text{O}_5$ on the factors reported in previous literatures that possibly alert the
377 processes of N_2O_5 uptake and ClNO_2 formation. We show that $\gamma\text{N}_2\text{O}_5$ highly correlated with the
378 ambient RH as well as liquid water content, confirming the critical role of water content in N_2O_5 uptake
379 and explained the reason why EJ05 had a good performance. The dependence of $\gamma\text{N}_2\text{O}_5$ on nitrate mass



380 concentration does not follow the rule of nitrate suppressing effect (Wahner et al., 1998), which may
381 be due to the covariance of nitrate and liquid water content. With respect to other factors, insignificant
382 impacts on the N_2O_5 uptake are obtained.



383
384 **Figure 5.** The inter-comparison of observation and parameterization of N_2O_5 uptake coefficient (a)
385 and ClNO_2 yield (b). The larger size of solid dots represents the median results. The parameterizations
386 of EJ05, BT09, Yu20 and BK97 cited from Evans and Jacob (2005), Bertram and Thornton (2009), Yu
387 et al. (2020), Behnke et al. (1997), respectively. The fitted ClNO_2 yield (colored by black) in panel (b)
388 shows the best fitting result in the study by adopting the k_4/k_3 of 32.0.

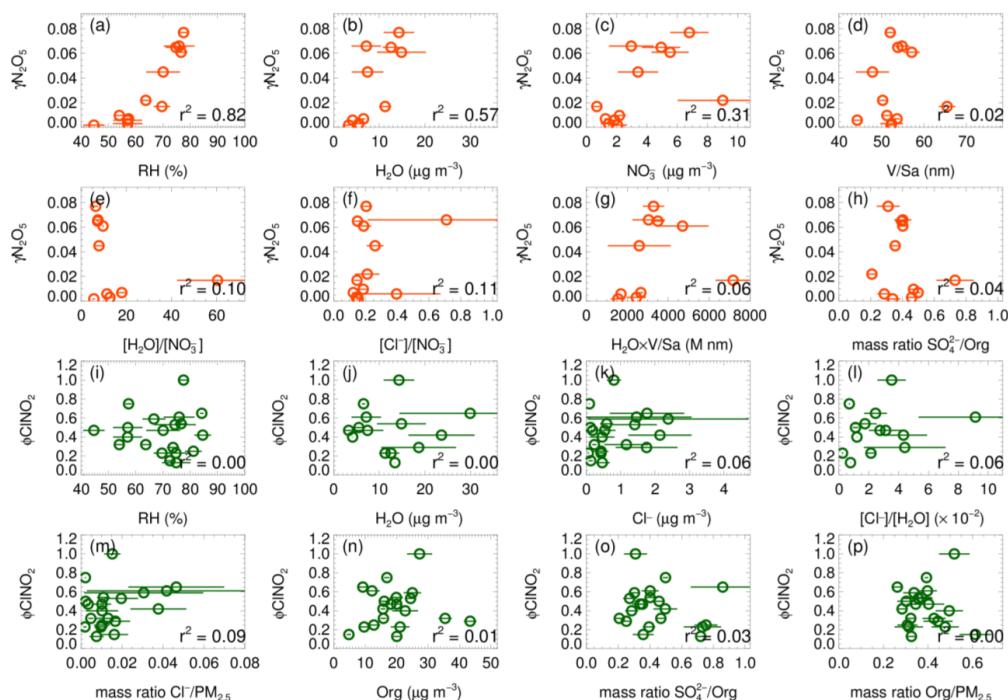
389 Bertram and Thornton (2009) also proposed a ClNO_2 yield parameterization method that
390 considering the ratio of ALWC and chloride content (Eq. 9), here the k_4/k_3 was the ratio of reaction
391 rate of H_2ONO_2^+ versus Cl^- to H_2O and adopted as 483 ± 175 . Behnke et al. (1997) determined this
392 ratio of 836 ± 32 , while it is estimated to be 105 ± 37 in Yu et al. (2020).

$$393 \quad \varphi_{\text{BT09}} = \left(\frac{[\text{H}_2\text{O}]}{1 + k_4/k_3[\text{Cl}^-]} \right)^{-1} \quad (9)$$

394 Figure 5(b) shows that all the predicting ClNO_2 yield based on the abovementioned parameterizations
395 overestimated the observations. The performance of the parameterization schemes of BK97 and BT09



396 based on the model aerosol conditions with an overestimation up to $\sim 100\%$ are expected and consistent
 397 with previous studies, which may be caused by the unaccounted potentially competitive effect of other
 398 species like organics, sulfate for the NO_2 intermediate (McDuffie et al., 2018a; Staudt et al., 2019; Xia
 399 et al., 2021; Wang et al., 2017d). Although the empirical parameterization (Yu20) based on field
 400 observations improved the prediction and narrowed the gap effectively, the overestimation is still large
 401 with an average of $\sim 50\%$, which indicated that the yield are more strongly suppressed than those
 402 observed in the campaigns of Yu et al. (2020). The factor 32.0 (k_4/k_3 in Eq. 9) was derived by iterative
 403 algorithms to achieve the best consistent between the observed and parameterized ClNO_2 yield, which
 404 is smaller than the Yu20 parameters by factors of 3.3. We examined the relationships of ClNO_2 yields
 405 with aerosol water content and other aerosol compositions as shown in Figure 6(i-p). We show that
 406 ϕClNO_2 only weakly correlated with the content of chloride (including the mass ratio and fraction in
 407 $\text{PM}_{2.5}$) and the molar ratio of chloride to water, confirmed the dependence found in laboratory studies.
 408 However, we did not find the dependence of the yields with aerosol organic or sulfate, as well as the
 409 RH and water alone in the campaign, implying the ClNO_2 yield mechanism is much more complicated
 410 than the laboratory conditions.



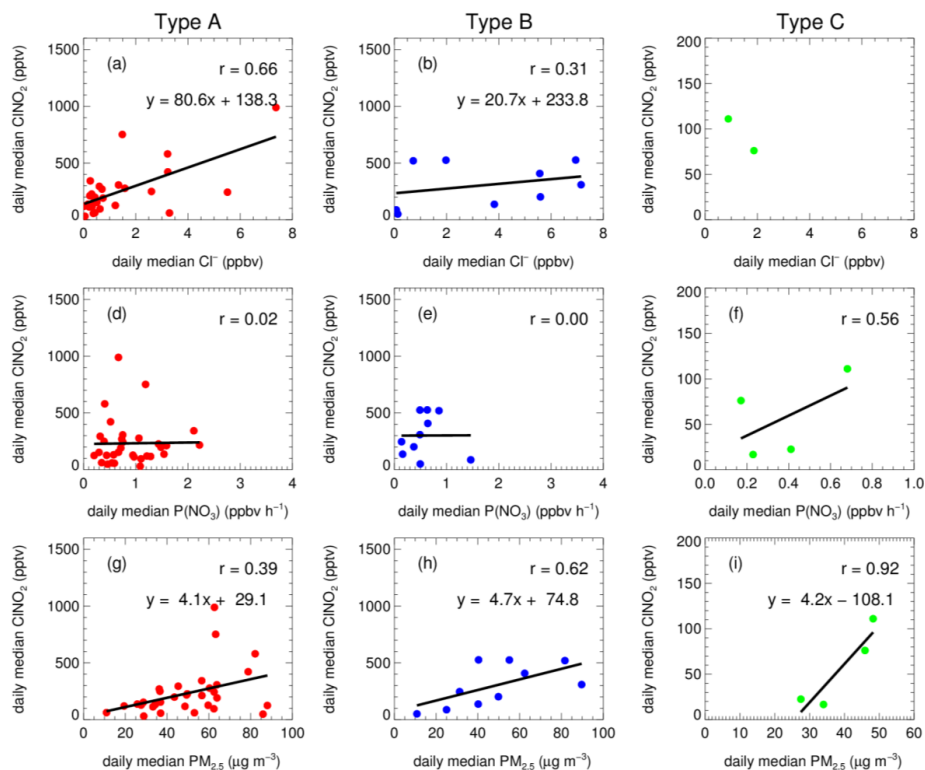
411

412 **Figure 6.** The estimated N_2O_5 uptake coefficient and ClNO_2 yield versus related parameters.



413 3.4 The factors influence ClNO₂ formation

414 The ClNO₂ formation can be largely affected by the budget of NO₃-N₂O₅ and N₂O₅ uptake processes.
415 The variation of NO₃ loss by VOC and NO alert the NO₃ loss distribution by N₂O₅ uptake and ClNO₂
416 formation indirectly. Figure 7 shows the correlation between daily median ClNO₂ and mass
417 concentration of chloride, PM_{2.5} and NO₃ production rate for the three types of air masses. Due to the
418 limited dataset of type C, the correlation analysis may not make sense, therefore, we did not take type
419 C into consideration in detailed discussion. We show that the mass concentration of chloride also
420 showed a correlation coefficient with ClNO₂ by 0.66 and 0.31 for type A and B, respectively.
421 Furthermore, the mass concentration of PM_{2.5} correlated reasonably with the ClNO₂ formation with
422 the correlation coefficient of 0.39 and 0.62 for type A and B, respectively. But, the levels of ClNO₂
423 demonstrate little relationship with the nitrate production rate. This is quite different from the results
424 observed in United Kingdom, where the ClNO₂ levels are mainly controlled by NO₂ and O₃, rather
425 than by the N₂O₅ uptake processes (Sommariva et al., 2018).



426
427 **Figure 7.** The functional dependence of daily median of ClNO₂ on particulate chloride, nitrate radical
428 production rate and PM_{2.5} in the air mass of Type A (a, d, g), Type B (b, e, h) and Type C (c, f, i).



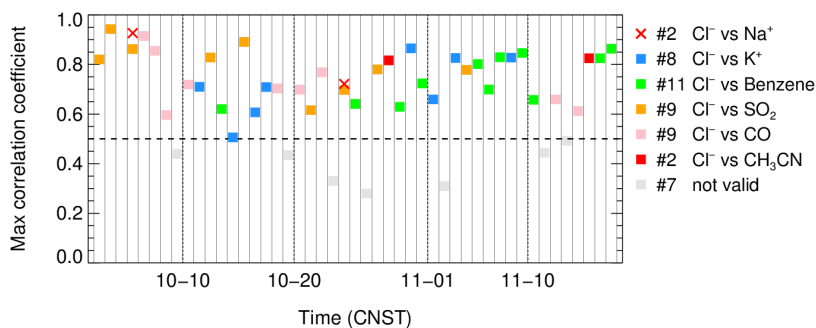
429 The low correlation between ClNO_2 and NO_3 production rate is within expectations. In general, the
430 production of nitrate radical controls the total budget of N_2O_5 , if N_2O_5 uptake dominated the sink of
431 NO_3 , as the result the N_2O_5 uptake and its products would show good correlation with NO_3 production
432 rate. But in fact, NO_3 loss can also be affected by other loss pathways, like the reactions with NO and
433 VOCs. In many cases, the NO_3 loss is dominated by VOC or NO , that means the ClNO_2 formation is
434 suppressed. If the two loss pathways are highly varied due to irregular emissions, then the relationship
435 between ClNO_2 and NO_3 production rate would be less correlated. We confirmed large variations of
436 NO and VOC (not shown) in hourly and daily scales, which means the proportion of N_2O_5 uptake to
437 the total loss of NO_3 is highly varied correspondingly. Overall, the low correlation in the study
438 indicated that the ClNO_2 formation through N_2O_5 uptake is not limited by NO_3 formation processes,
439 at least in Type A and B. With respect to the air mass Type C, ClNO_2 showed correlation with $\text{P}(\text{NO}_3)$
440 with the correlation coefficient of 0.56.

441 As the precursor of ClNO_2 , higher concentrations of particulate chloride result in high ClNO_2 yield
442 from N_2O_5 uptake to some extent, as evidenced by our field observation (Figure 6) and previous
443 laboratory studies (Bertram and Thornton, 2009; Roberts et al., 2009; Ryder et al., 2015). High $\text{PM}_{2.5}$
444 concentrations usually provide more aerosol surface area to promote N_2O_5 uptake. The close
445 relationship between ClNO_2 and $\text{PM}_{2.5}$ indicate that aerosol surface area, most likely, is a critical factor
446 that limited ClNO_2 formation. The proportion of nitrate in the total $\text{PM}_{1.0}$ was small with an average
447 of 10.4%, therefore the correlation of ClNO_2 and $\text{PM}_{2.5}$ cannot attribute to the covariance between
448 nitrate and $\text{PM}_{2.5}$. In addition, the ClNO_2 level in the air mass of Type B show higher correlation to
449 both Cl^- and $\text{PM}_{2.5}$ than type A, suggesting that the ClNO_2 formation in Type B is more effectively
450 affected by the levels of chloride and $\text{PM}_{2.5}$.

451 Recently model simulation indicated that the ClNO_2 chemistry level is sensitive to the emission of
452 chloride in PRD (Li et al., 2021). In this study, a question raised that where is the source of chloride?
453 The mass ratio of Cl^-/Na^+ is often used as an indicator of sea salt or anthropogenic sources to chloride
454 with a threshold of 1.81 (Yang et al., 2018; Wang et al., 2016). High ratio means the particulate chloride
455 affected by anthropogenic emission rather than sea salt. We determine that the mean mass ratios of Cl^-
456 to Na^+ are 5.3, 6.3 and 3.1 in Type A, B and C, respectively (Figure 3). This indicated that $\text{PM}_{2.5}$
457 sampled during the campaign was not strongly influenced by fresh sea salt aerosols. In the three types,
458 the Type C air mass had a lowest ratio and may be influenced by both sea salt and anthropogenic
459 emissions, which seems reasonable since it come from South China Sea. If we assume that Type A air
460 mass is free of sea salt and only influenced by anthropogenic activities, the higher ratio implies more
461 intensive chloride source in Type B. The correlation between particulate chloride and some possible
462 indicators, including K^+ , benzene, SO_2 , CO , acetonitrile (CH_3CN), were examined day by day. Figure



463 8 shows the max correlation coefficient (R^2) in each day with a threshold of 0.5. We filtered out 39 out
 464 of 46 days during this campaign with a fraction of 85%. Among the 39 days, a total of 11 days is
 465 associated with strongest correlation between Cl^- and benzene, which is typically come from industrial
 466 emissions. Cl^- also correlated with K^+ , CO and CH_3CN in 19 day in total, implies potential
 467 contributions from biomass burning emissions. In total of 9 days for highest correlations of Cl^- with
 468 SO_2 indicated power plants emissions may also contributed to Cl^- emission. We summarized that the
 469 source of chloride may be highly varied from different anthropogenic activities including biomass
 470 burning, industrial processes as well as power plants. The statistic results in Table 5 suggest that the
 471 Cl^- in air mass of Type A were affected by various sources, especially related to the sources associated
 472 with K^+ , benzene and CH_3CN ; the Cl^- in Type B was mainly contributed by the similar source of CO,
 473 and Type C was only affected by power plants emissions. In addition, Figure 8 showed that there are
 474 2 days that the correlations between Cl^- and Na^+ exceeded the max of the selected anthropogenic factor
 475 matrix, indicated that the aerosol still also impacted by sea salt to some extent.



476
 477 **Figure 8.** The max correlation coefficient between particulate chloride and a selected parameter matrix
 478 (including K^+ , benzene, SO_2 , CO, acetonitrile (CH_3CN)) in each day. The labelled number in each
 479 legend indicates the days be the maximum, the dashed line denotes the threshold of 0.5 (39 valid days
 480 out of 46 in total). The cross means the correlation coefficient between Cl^- and Na^+ is larger than the
 481 max.

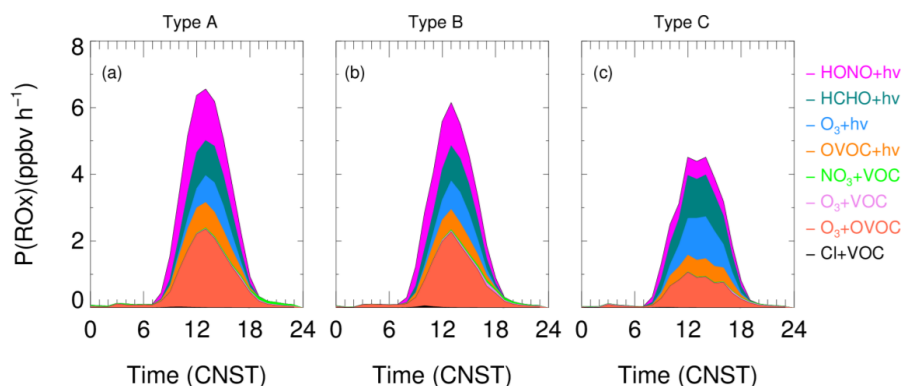
482 **Table 5.** The statistic of the days for highest factors correlated with particulate chloride in different
 483 air mass pattern.

factors	Type A	Type B	Type C
K^+	8	0	0
Benzene	9	2	0
SO_2	5	1	3
CO	4	5	0
CH_3CN	2	0	0



484 3.5 The impacts of ClNO₂ on atmospheric oxidation

485 In this section, we focus on the assessment of the impact of ClNO₂ photolysis on the source of radicals
486 and the contribution to the atmospheric oxidation. Figure 9 shows the diurnal accumulation of ROx
487 production rate from model simulations with ClNO₂ chemistry in the three types of air mass. The total
488 ROx production rate was higher in Type A and then followed by Type B and C, in which photolysis of
489 HONO, HCHO, O₃ and OVOCs had large contributions. Cl radical, liberated by ClNO₂, enhanced
490 little ROx production, with a morning peak contribution of 1.3%, 2.2% and 1.8% for Type A, B, C,
491 respectively (08:00-09:00). The contribution of ClNO₂ photolysis to the production of ROx is less than
492 1% on daytime averaged, similar to the results obtained in winter Shanghai (Lou et al., 2022) as well
493 as North China (Xia et al., 2021), and much lower compared to previous studies reported in summer
494 time in both north and south China (Tan et al., 2017; Wang et al., 2016; Tham et al., 2016). In addition,
495 we noticed that the significant role of OVOCs (including photolysis and reacts with O₃) in producing
496 ROx at this site, especially in the Type A and B air mass. This result is consistent with that constrained
497 by observed OVOCs in Guangzhou City (Wang et al., 2022c).

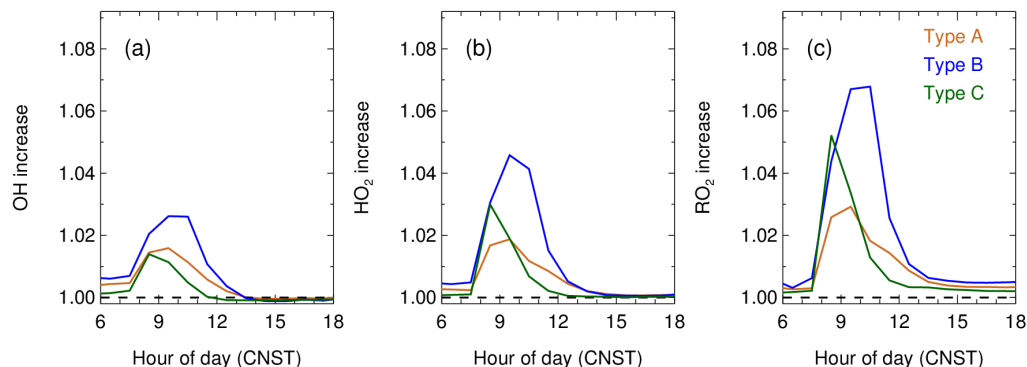


498
499 **Figure 9.** The diurnal cycle and distribution of ROx production rate in the three types air masses.

500 Figure 10 shows the enhancement of OH, HO₂ and RO₂ radicals with the consideration of ClNO₂
501 chemistry. The enhancement of the three radicals peaked in the morning. On average, OH
502 concentration was enhanced by 1.5% to 2.6% in different air masses. The percentage of enhancement
503 for HO₂ radical was 1.9% to 4.6%, whereas the enhancement for RO₂ was a little bit higher (3.0% to
504 6.8%). In general, the enhancement of radicals was more significant in Type B than other two types of
505 air masses, which is related to elevated ClNO₂ concentrations for these air masses. Low ClNO₂ and
506 other radical precursors led to an earlier enhancement peak (08:00-09:00) in Type C and lasted a short
507 time period. Although the increase peak occurred later at 09:00-10:00 for the air mass of Type A and

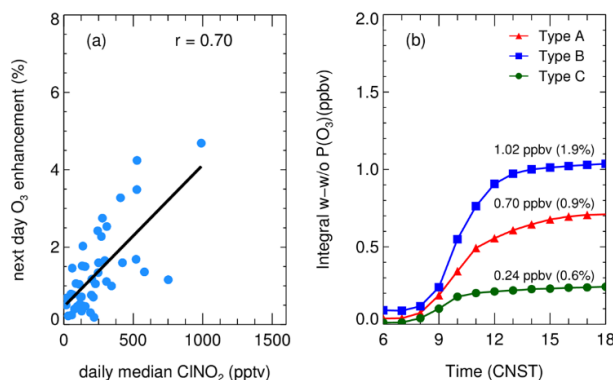


508 Type B, the increase lasted for a longer time and had a longer effect. Overall, daytime OH, HO₂ and
509 RO₂ enhanced by 1.0%, 2.0%, and 3.0% on campaign average.



510
511 **Figure 10.** The diurnal cycle on the enhancement of OH (a), HO₂ (b), RO₂ (c) by ClNO₂ chemistry in
512 the three air mass patterns.

513 Figure 11 depicts the integral enhancement of O₃ production by ClNO₂ photolysis varied from less
514 than 0.1 ppbv to 4 ppbv day by day, with a percentage of <1% to 4.9% with a median of 0.8%. Our results
515 are comparable with the winter case in North China (Xia et al., 2021). The next day O₃ enhancement
516 was highly correlated with the level of ClNO₂ with the correlation coefficient of 0.7. The net O₃
517 production enhanced by 0.70 ppbv h⁻¹ (0.9%), 1.02 ppbv h⁻¹ (1.9%), 0.24 ppbv h⁻¹ (0.6%) on daytime
518 accumulation in Type A, B, C, respectively, which is consistent with the nocturnal level of ClNO₂ in
519 the three air masses presented in Table 3.



520
521 **Figure 11.** (a) The correlation of daily median ClNO₂ (18:00-06:00) and its impact on next day net O₃
522 production enhancement during the campaign; (b) the average contribution of daytime integral O₃ by
523 ClNO₂ mechanism in the three types of air masses.



524 Previous studies suggest that chlorine radicals from ClNO₂ photolysis may contribute significantly
525 to the oxidation of some VOCs species, especially for long-chain alkanes (Shi et al., 2020; Wang et al.,
526 2022b). The oxidation of long-chain alkanes (C₁₀~14 n-alkanes) by chloride and OH radicals during
527 the morning hour (08:00 - 09:00) were also evaluated based on modeled oxidants concentration. We
528 observe small contributions of chloride radical with a percentage of 3.2%, 3.7% and 4.2% for n-decane,
529 n-dodecane and n-tetradecane, respectively. The contributions reduced to <1% on daytime average.
530 We also checked the role of chloride in short-chain alkanes oxidation, obtaining an even smaller
531 contribution than the long-chain alkanes. Therefore, we concluded that, chloride radicals liberated by
532 ClNO₂ photolysis, is not critical to the oxidation of alkanes compared with OH oxidation during the
533 campaign. We note that several studies reported other sources produced large amount of chloride
534 radicals like Cl₂ (Liu et al., 2017; Xia et al., 2020), BrCl (Peng et al., 2021), the daytime reaction of
535 HCl with OH (Riedel et al., 2012; Eger et al., 2019; Li et al., 2019). However, it is not possible to assess
536 the overall impacts by constraining all precursors of chloride radical, which may warrant further
537 investigation by more comprehensive field studies equipped with the instruments for detecting these
538 species.

539 4. Conclusion

540 An intensive field study in Pearl River Delta took place during a photochemical pollution season from
541 Sept. 26th to Nov. 17th, 2019, providing a comprehensive observation dataset to understand the ClNO₂
542 chemistry and its impacts on the air quality. We found that the air masses highly varied from different
543 regions and divided in three types according to the results of backward trajectory. Two of them, air
544 mass from northern and northeastern inland cities and the eastern coastal regions, features polluted
545 with elevated O₃ and related trace gases like NO_x and CO. Correlation analysis showed that ClNO₂
546 formation is limited by chloride availability and PM_{2.5} concentrations (mostly due to aerosol surface
547 area) at this site. In general, we observed a wide variation for determining factors of ClNO₂ formation
548 in different kinds of air masses.

549 We estimated the N₂O₅ uptake coefficients and ClNO₂ yield during this campaign and assessed the
550 performance of previous parameterizations schemes. The newly developed observation-based
551 empirical parameterization was also checked and showed an overall underestimation. We showed the
552 γ_{N₂O₅} only strongly correlated with RH, and the parameterization proposed by Evans and Jacob (2005)
553 showed a considerable consistent with the observation. The ClNO₂ yield only showed weak correlation
554 with the content of particle chloride, and the exist parameterizations systematically overestimated the
555 yield.

556 The particulate chloride mainly originated from anthropogenic emissions rather than sea salt.



557 However, the specific contributing source of chloride in this region cannot be determined, due to the
558 varying correlation relationship with different kinds of anthropogenic emission indicators day by day.
559 We can only infer that the air mass of Type A affected by most complicated anthropogenic emissions
560 including biomass burning, power plants as well as the even possible usage of industrial solvents. This
561 result highlights the ClNO₂ chemistry may be triggered by many kinds of anthropogenic activities in
562 the PRD regions (Wang et al., 2016; Yang et al., 2018). The sources of particulate chloride warrant
563 further detailed exploration using the dataset along with other observations in this region.

564 In the end, we investigate the impacts of ClNO₂ chemistry on atmospheric oxidation by a box model.
565 It is demonstrated that chloride radicals liberated by ClNO₂ chemistry had a relatively small
566 contribution to the following daytime level of OH, HO₂, and RO₂ radicals, as well as a small
567 enhancement of O₃ and ROx production in all the three types of air masses. The impacts of ClNO₂
568 chemistry were larger in the Type B than that of Type A. Overall, the small contribution of ClNO₂
569 chemistry in PRD region may be due to the limited ClNO₂ produced by N₂O₅ uptake processes, and
570 other strong primary sources of radicals weakened its contribution indirectly. Given complex source
571 of particulate chloride, we call for more field investigations to address the chloride chemistry and its
572 roles in air pollutions in China.

573 **Data availability.** The datasets used in this study are available from the corresponding author upon
574 request (byuan@jnu.edu.cn).

575 **Author contributions.** H.C.W. and B.Y. designed the study. E.Z, X.X.Z. and H.C.W. operated and
576 calibrated the CIMS, H.C.W. analyzed the data, H.C.W. and B.Y. wrote the manuscript with inputs
577 from all coauthors.

578 **Competing interests.** The authors declare that they have no conflicts of interest.

579 **Acknowledgements.** This work was supported by the National Natural Science Foundation of China
580 (grant No. 41877302, 42175111, 42121004), Guangdong Natural Science Funds for Distinguished
581 Young Scholar (grant No. 2018B030306037), Key-Area Research and Development Program of
582 Guangdong Province (grant No. 2019B110206001), and Guangdong Innovative and Entrepreneurial
583 Research Team Program (grant No. 2016ZT06N263). This work was also supported by Special Fund
584 Project for Science and Technology Innovation Strategy of Guangdong Province (Grant
585 No.2019B121205004). The authors gratefully acknowledge the Jinan University science team for their



586 technical support and discussions during this campaign. We thank for the NOAA Air Resources
587 Laboratory for providing the HYSPLIT model.

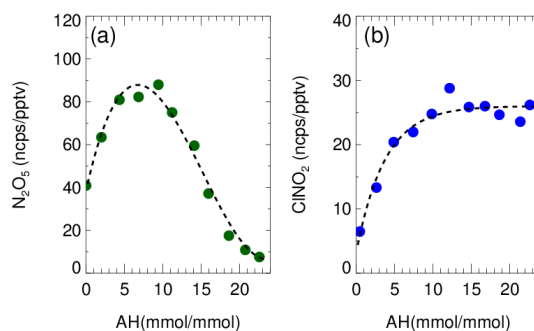
588 **Appendix**

589 **A1. The calibration of CIMS**

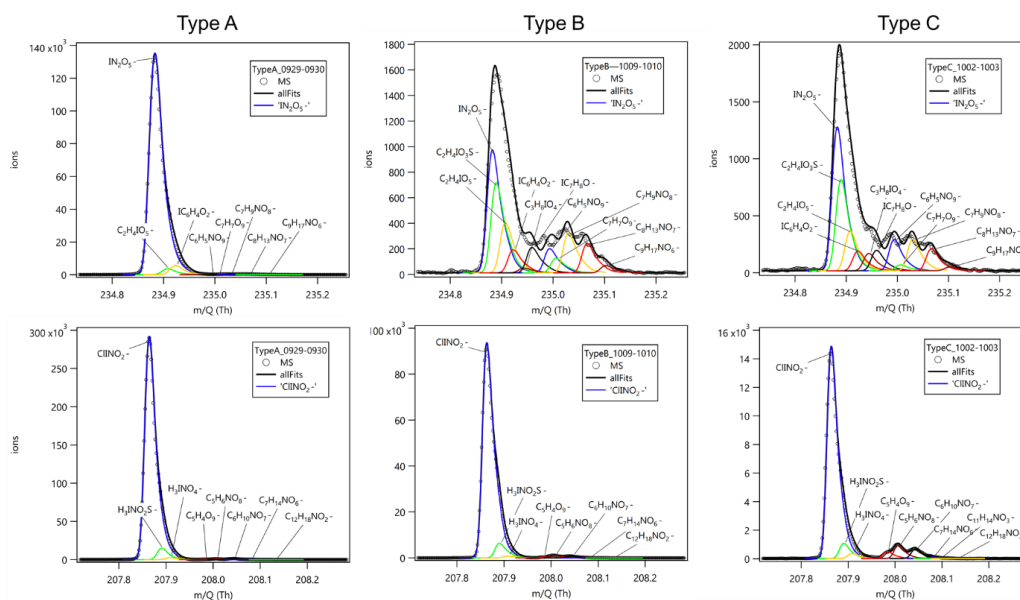
590 The calibration of ClNO₂ measurement sensitivity has been introduced in Wang et al. (2022a). In brief,
591 a nitrogen flow (6 mL min⁻¹) containing 10 ppmv Cl₂ was passed over a slurry containing NaNO₂ and
592 NaCl to produce ClNO₂ (Thaler et al., 2011), and NaCl was included in the slurry in order to minimize
593 the formation of NO₂ as a byproduct. The mixed flow containing ClNO₂ was then conditioned to a
594 given RH and sampled into the CIMS instrument. To quantify ClNO₂, the mixed flow was delivered
595 directly into a cavity attenuated phase shift spectroscopy instrument (CAPS, Model N500, Teledyne
596 API) to measure background NO₂ concentrations or through a thermal dissociation tube at 365 °C to
597 fully decompose ClNO₂ to NO₂, and the total NO₂ concentrations were then determined using CAPS.
598 The differences in the measured NO₂ concentrations with and without thermal dissociation was
599 equivalent to ClNO₂ concentrations. The CAPS instrument had a detection limit of 0.2 ppbv in 1 min
600 for NO₂ and an uncertainty of ~10%. To calibrate CIMS measurements of N₂O₅, a humidity adjustable
601 mixed flow containing stable N₂O₅, which was produced via O₃ oxidation of NO₂, was sampled into
602 the CIMS instrument to obtain a normalized humidity dependence curve of N₂O₅. While the
603 concentration of N₂O₅ source is not quantified due to the absence of a N₂O₅ detector, so we delivered
604 the N₂O₅ source flow through a supersaturated sodium chloride solution to convert N₂O₅ to ClNO₂
605 with a unit efficiency at 50% RH, which is a widely used method for the calibration of ClNO₂ by CIMS
606 technique. The absolute N₂O₅ sensitivity at RH 50% can be realized and then scaled to other humidity
607 condition by the normalized N₂O₅ sensitivity curve determined before. The sensitivity curves for N₂O₅
608 and ClNO₂ to water content were shown in Figure A1. Figure A2 shows the high-resolution peak fitting
609 results of typical mass spectra at m/z 235 and m/z 208 for N₂O₅ and ClNO₂ in three air mass patterns,
610 respectively. The peaks of N₂O₅ and ClNO₂ were clearly resolved in the mass spectra. The peak of
611 IN₂O₅⁻ can be well retrieved by separating a large adjacent peak of C₂H₄IO₃S⁻ in the air masses affected
612 by marine emissions (Type B and C), which might be hydroperoxymethyl thioformate (HPMTF) from
613 dimethyl sulfide oxidation (Veres et al., 2020). The interference signals including H₃INO₂S⁻ for ClNO₂



614 measurements can also be well separated in all the three air mass patterns. These results underline the
 615 necessity and feasibility in the application of ToF analyzer in detecting N_2O_5 and $ClNO_2$ with iodide
 616 CIMS.



617
 618 **Figure A1.** CIMS sensitivities as a function of water concentration for (a) N_2O_5 and (b) $ClNO_2$.



619
 620 **Figure A2.** Cases of high-resolution spectra fitting for N_2O_5 and $ClNO_2$ by ToF-CIMS under three air
 621 mass patterns.

622

623 Reference

624 Anttila, T., Kiendler-Scharr, A., Tillmann, R., and Mentel, T. F.: On the reactive uptake of gaseous
 625 compounds by organic-coated aqueous aerosols: Theoretical analysis and application to the
 626 heterogeneous hydrolysis of N_2O_5 , *J Phys Chem A*, 110, 10435-10443, Doi 10.1021/Jp062403c, 2006.



- 627 Atkinson, R., and Arey, J.: Atmospheric degradation of volatile organic compounds, *Chem Rev*, 103,
628 4605-4638, 10.1021/cr0206420, 2003.
- 629 Atkinson, R., Baulch, D. L., Cox, R. A., Crowley, J. N., Hampson, R. F., Hynes, R. G., Jenkin, M. E.,
630 Rossi, M. J., and Troe, J.: Evaluated kinetic and photochemical data for atmospheric chemistry:
631 Volume II - gas phase reactions of organic species, *Atmospheric Chemistry and Physics*, 6, 3625-4055,
632 DOI 10.5194/acp-6-3625-2006, 2006.
- 633 Bannan, T. J., Booth, A. M., Bacak, A., Muller, J. B. A., Leather, K. E., Le Breton, M., Jones, B., Young,
634 D., Coe, H., Allan, J., Visser, S., Slowik, J. G., Furger, M., Prevot, A. S. H., Lee, J., Dunmore, R. E.,
635 Hopkins, J. R., Hamilton, J. F., Lewis, A. C., Whalley, L. K., Sharp, T., Stone, D., Heard, D. E., Fleming,
636 Z. L., Leigh, R., Shallcross, D. E., and Percival, C. J.: The first UK measurements of nitryl chloride
637 using a chemical ionization mass spectrometer in central London in the summer of 2012, and an
638 investigation of the role of Cl atom oxidation, *Journal of Geophysical Research-Atmospheres*, 120,
639 5638-5657, 10.1002/2014jd022629, 2015.
- 640 Bannan, T. J., Bacak, A., Le Breton, M., Flynn, M., Ouyang, B., McLeod, M., Jones, R., Malkin, T. L.,
641 Whalley, L. K., Heard, D. E., Bandy, B., Khan, M. A. H., Shallcross, D. E., and Percival, C. J.: Ground
642 and Airborne UK Measurements of Nitryl Chloride: An Investigation of the Role of Cl Atom Oxidation
643 at Weybourne Atmospheric Observatory, *Journal of Geophysical Research-Atmospheres*, 122, 11154-
644 11165, 10.1002/2017jd026624, 2017.
- 645 Bannan, T. J., Khan, M. A. H., Le Breton, M., Priestley, M., Worrall, S. D., Bacak, A., Marsden, N. A.,
646 Lowe, D., Pitt, J., Shallcross, D. E., and Percival, C. J.: A Large Source of Atomic Chlorine From
647 ClNO₂ Photolysis at a UK Landfill Site, *Geophysical Research Letters*, 46, 8508-8516,
648 10.1029/2019gl083764, 2019.
- 649 Behnke, W., George, C., Scheer, V., and Zetzsch, C.: Production and decay of ClNO₂, from the reaction
650 of gaseous N₂O₅ with NaCl solution: Bulk and aerosol experiments, *Journal of Geophysical Research-*
651 *Atmospheres*, 102, 3795-3804, Doi 10.1029/96jd03057, 1997.
- 652 Bertram, T. H., and Thornton, J. A.: Toward a general parameterization of N₂O₅ reactivity on aqueous
653 particles: the competing effects of particle liquid water, nitrate and chloride, *Atmospheric Chemistry*
654 *and Physics*, 9, 8351-8363, 2009.
- 655 Bohn, B., Corlett, G. K., Gillmann, M., Sanghavi, S., Stange, G., Tensing, E., Vrekoussis, M., Bloss,
656 W. J., Clapp, L. J., Kortner, M., Dorn, H. P., Monks, P. S., Platt, U., Plass-Dulmer, C., Mihalopoulos,
657 N., Heard, D. E., Clemitshaw, K. C., Meixner, F. X., Prevot, A. S. H., and Schmitt, R.: Photolysis
658 frequency measurement techniques: results of a comparison within the ACCENT project, *Atmospheric*
659 *Chemistry and Physics*, 8, 5373-5391, 2008.
- 660 Brown, S. S., Stark, H., and Ravishankara, A. R.: Applicability of the steady state approximation to
661 the interpretation of atmospheric observations of NO₃ and N₂O₅, *Journal of Geophysical Research-*
662 *Atmospheres*, 108, Artn 4539
663 Doi 10.1029/2003jd003407, 2003.
- 664 Brown, S. S., Ryerson, T. B., Wollny, A. G., Brock, C. A., Peltier, R., Sullivan, A. P., Weber, R. J.,
665 Dube, W. P., Trainer, M., Meagher, J. F., Fehsenfeld, F. C., and Ravishankara, A. R.: Variability in
666 nocturnal nitrogen oxide processing and its role in regional air quality, *Science*, 311, 67-70, DOI
667 10.1126/science.1120120, 2006.
- 668 Brown, S. S., and Stutz, J.: Nighttime radical observations and chemistry, *Chem Soc Rev*, 41, 6405-



- 669 6447, Doi 10.1039/C2cs35181a, 2012.
- 670 Brown, S. S., Dube, W. P., Tham, Y. J., Zha, Q. Z., Xue, L. K., Poon, S., Wang, Z., Blake, D. R., Tsui,
671 W., Parrish, D. D., and Wang, T.: Nighttime chemistry at a high altitude site above Hong Kong, Journal
672 of Geophysical Research-Atmospheres, 121, 2457-2475, 10.1002/2015jd024566, 2016.
- 673 Chen, X., Wang, H., Lu, K., Li, C., Zhai, T., Tan, Z., Ma, X., Yang, X., Liu, Y., Chen, S., Dong, H., Li,
674 X., Wu, Z., Hu, M., Zeng, L., and Zhang, Y.: Field Determination of Nitrate Formation Pathway in
675 Winter Beijing, Environmental Science & Technology, 54, 9243-9253, 10.1021/acs.est.0c00972, 2020.
- 676 Chen, X., Wang, H., and Lu, K.: Interpretation of NO₃-N₂O₅ observation via steady state in high-
677 aerosol air mass: the impact of equilibrium coefficient in ambient conditions, Atmos. Chem. Phys., 22,
678 3525-3533, 10.5194/acp-22-3525-2022, 2022.
- 679 Clegg, S. L., Brimblecombe, P., and Wexler, A. S.: Thermodynamic model of the system H⁺-NH₄⁺-
680 SO₄²⁻-NO₃⁻-H₂O at tropospheric temperatures, J Phys Chem A, 102, 2137-2154, DOI
681 10.1021/jp973042r, 1998.
- 682 DeCarlo, P. F., Kimmel, J. R., Trimborn, A., Northway, M. J., Jayne, J. T., Aiken, A. C., Gonin, M.,
683 Fuhrer, K., Horvath, T., Docherty, K. S., Worsnop, D. R., and Jimenez, J. L.: Field-deployable, high-
684 resolution, time-of-flight aerosol mass spectrometer, Analytical Chemistry, 78, 8281-8289,
685 10.1021/ac061249n, 2006.
- 686 Dong, H. B., Zeng, L. M., Hu, M., Wu, Y. S., Zhang, Y. H., Slanina, J., Zheng, M., Wang, Z. F., and
687 Jansen, R.: Technical Note: The application of an improved gas and aerosol collector for ambient air
688 pollutants in China, Atmospheric Chemistry and Physics, 12, 10519-10533, 10.5194/acp-12-10519-
689 2012, 2012.
- 690 Eger, P. G., Friedrich, N., Schuladen, J., Shenolikar, J., Fischer, H., Tadic, I., Harder, H., Martinez, M.,
691 Rohloff, R., Tauer, S., Drewnick, F., Fachinger, F., Brooks, J., Darbyshire, E., Sciare, J., Pikridas, M.,
692 Lelieveld, J., and Crowley, J. N.: Shipborne measurements of ClNO₂ in the Mediterranean Sea and
693 around the Arabian Peninsula during summer, Atmospheric Chemistry and Physics, 19, 12121-12140,
694 10.5194/acp-19-12121-2019, 2019.
- 695 Evans, M. J., and Jacob, D. J.: Impact of new laboratory studies of N₂O₅ hydrolysis on global model
696 budgets of tropospheric nitrogen oxides, ozone, and OH, Geophysical Research Letters, 32, Artn
697 L09813
698 Doi 10.1029/2005gl022469, 2005.
- 699 Faxon, C. B., Bean, J. K., and Hildebrandt Ruiz, L.: Inland Concentrations of Cl₂ and ClNO₂ in
700 Southeast Texas Suggest Chlorine Chemistry Significantly Contributes to Atmospheric Reactivity,
701 Atmosphere, 6, 1487-1506, 10.3390/atmos6101487, 2015.
- 702 Finlaysonpitts, B. J., Ezell, M. J., and Pitts, J. N.: Formation of Chemically Active Chlorine
703 Compounds by Reactions of Atmospheric NaCl Particles with Gaseous N₂O₅ and ClONO₂, Nature, 337,
704 241-244, Doi 10.1038/337241a0, 1989.
- 705 Gaston, C. J., Thornton, J. A., and Ng, N. L.: Reactive uptake of N₂O₅ to internally mixed inorganic
706 and organic particles: the role of organic carbon oxidation state and inferred organic phase separations,
707 Atmospheric Chemistry and Physics, 14, 5693-5707, 10.5194/acp-14-5693-2014, 2014.
- 708 Ghosh, B., Papanastasiou, D. K., Talukdar, R. K., Roberts, J. M., and Burkholder, J. B.: Nitryl Chloride
709 (ClNO₂): UV/Vis Absorption Spectrum between 210 and 296 K and O(P-3) Quantum Yield at 193
710 and 248 nm, J Phys Chem A, 116, 5796-5805, 10.1021/jp207389y, 2012.



- 711 Hallquist, M., Stewart, D. J., Stephenson, S. K., and Cox, R. A.: Hydrolysis of N₂O₅ on sub-micron
712 sulfate aerosols, *Phys Chem Chem Phys*, 5, 3453-3463, Doi 10.1039/B301827j, 2003.
- 713 Haskins, J. D., Lee, B. H., Lopez-Hilifiker, F. D., Peng, Q. Y., Jaegle, L., Reeves, J. M., Schroder, J.
714 C., Campuzano-Jost, P., Fibiger, D., McDuffie, E. E., Jimenez, J. L., Brown, S. S., and Thornton, J. A.:
715 Observational Constraints on the Formation of Cl-2 From the Reactive Uptake of ClNO₂ on Aerosols
716 in the Polluted Marine Boundary Layer, *Journal of Geophysical Research-Atmospheres*, 124, 8851-
717 8869, 10.1029/2019jd030627, 2019.
- 718 He, X., Yuan, B., Wu, C., Wang, S., Wang, C., Huangfu, Y., Qi, J., Ma, N., Xu, W., Wang, M., Chen,
719 W., Su, H., Cheng, Y., and Shao, M.: Volatile organic compounds in wintertime North China Plain:
720 Insights from measurements of proton transfer reaction time-of-flight mass spectrometer (PTR-ToF-
721 MS), *Journal of Environmental Sciences*, 114, 98-114, <https://doi.org/10.1016/j.jes.2021.08.010>, 2022.
- 722 Jeong, D., Seco, R., Gu, D., Lee, Y., Nault, B. A., Knot, C. J., McGee, T., Sullivan, J. T., Jimenez, J.
723 L., Campuzano-Jost, P., Blake, D. R., Sanchez, D., Guenther, A. B., Tanner, D., Huey, L. G., Long, R.,
724 Anderson, B. E., Hall, S. R., Ullmann, K., Shin, H., Herndon, S. C., Lee, Y., Kim, D., Ahn, J., and Kim,
725 S.: Integration of airborne and ground observations of nitryl chloride in the Seoul metropolitan area
726 and the implications on regional oxidation capacity during KORUS-AQ 2016, *Atmos. Chem. Phys.*,
727 19, 12779-12795, 10.5194/acp-19-12779-2019, 2019.
- 728 Le Breton, M., Hallquist, A. M., Pathak, R. K., Simpson, D., Wang, Y. J., Johansson, J., Zheng, J.,
729 Yang, Y. D., Shang, D. J., Wang, H. C., Liu, Q. Y., Chan, C., Wang, T., Bannan, T. J., Priestley, M.,
730 Percival, C. J., Shallcross, D. E., Lu, K. D., Guo, S., Hu, M., and Hallquist, M.: Chlorine oxidation of
731 VOCs at a semi-rural site in Beijing: significant chlorine liberation from ClNO₂ and subsequent gas-
732 and particle-phase Cl-VOC production, *Atmospheric Chemistry and Physics*, 18, 13013-13030,
733 10.5194/acp-18-13013-2018, 2018.
- 734 Li, Q., Fu, X., Peng, X., Wang, W., Badia, A., Fernandez, R. P., Cuevas, C. A., Mu, Y., Chen, J., Jimenez,
735 J. L., Wang, T., and Saiz-Lopez, A.: Halogens Enhance Haze Pollution in China, *Environmental
736 Science & Technology*, 55, 13625-13637, 10.1021/acs.est.1c01949, 2021.
- 737 Li, Q. Y., Zhang, L., Wang, T., Tham, Y. J., Ahmadov, R., Xue, L. K., Zhang, Q., and Zheng, J. Y.:
738 Impacts of heterogeneous uptake of dinitrogen pentoxide and chlorine activation on ozone and reactive
739 nitrogen partitioning: improvement and application of the WRF-Chem model in southern China,
740 *Atmospheric Chemistry and Physics*, 16, 14875-14890, 10.5194/acp-16-14875-2016, 2016.
- 741 Li, Q. Y., Borge, R., Sarwar, G., de la Paz, D., Gantt, B., Domingo, J., Cuevas, C. A., and Saiz-Lopez,
742 A.: Impact of halogen chemistry on summertime air quality in coastal and continental Europe:
743 application of the CMAQ model and implications for regulation, *Atmospheric Chemistry and Physics*,
744 19, 15321-15337, 10.5194/acp-19-15321-2019, 2019.
- 745 Liu, X. G., Gu, J. W., Li, Y. P., Cheng, Y. F., Qu, Y., Han, T. T., Wang, J. L., Tian, H. Z., Chen, J., and
746 Zhang, Y. H.: Increase of aerosol scattering by hygroscopic growth: Observation, modeling, and
747 implications on visibility, *Atmospheric Research*, 132, 91-101, 10.1016/j.atmosres.2013.04.007, 2013.
- 748 Liu, X. X., Qu, H., Huey, L. G., Wang, Y. H., Sjostedt, S., Zeng, L. M., Lu, K. D., Wu, Y. S., Ho, M.,
749 Shao, M., Zhu, T., and Zhang, Y. H.: High Levels of Daytime Molecular Chlorine and Nitryl Chloride
750 at a Rural Site on the North China Plain, *Environmental Science & Technology*, 51, 9588-9595,
751 10.1021/acs.est.7b03039, 2017.
- 752 Lou, S., Tan, Z., Gan, G., Chen, J., Wang, H., Gao, Y., Huang, D., Huang, C., Li, X., Song, R., Wang,



- 753 H., Wang, M., Wang, Q., Wu, Y., and Huang, C.: Observation based study on atmospheric oxidation
754 capacity in Shanghai during late-autumn: Contribution from nitryl chloride, *Atmospheric Environment*,
755 271, 10.1016/j.atmosenv.2021.118902, 2022.
- 756 McDuffie, E. E., Fibiger, D. L., Dube, W. P., Hilfiker, F. L., Lee, B. H., Jaegle, L., Guo, H. Y., Weber,
757 R. J., Reeves, J. M., Weinheimer, A. J., Schroder, J. C., Campuzano-Jost, P., Jimenez, J. L., Dibb, J. E.,
758 Veres, P., Ebben, C., Sparks, T. L., Wooldridge, P. J., Cohen, R. C., Campos, T., Hall, S. R., Ullmann,
759 K., Roberts, J. M., Thornton, J. A., and Brown, S. S.: ClNO₂ Yields From Aircraft Measurements
760 During the 2015 WINTER Campaign and Critical Evaluation of the Current Parameterization, *Journal*
761 *of Geophysical Research-Atmospheres*, 123, 12994-13015, 10.1029/2018JD029358, 2018a.
- 762 McDuffie, E. E., Fibiger, D. L., Dube, W. P., Lopez-Hilfiker, F., Lee, B. H., Thornton, J. A., Shah, V.,
763 Jaegle, L., Guo, H. Y., Weber, R. J., Reeves, J. M., Weinheimer, A. J., Schroder, J. C., Campuzano-Jost,
764 P., Jimenez, J. L., Dibb, J. E., Veres, P., Ebben, C., Sparks, T. L., Wooldridge, P. J., Cohen, R. C.,
765 Hornbrook, R. S., Apel, E. C., Campos, T., Hall, S. R., Ullmann, K., and Brown, S. S.: Heterogeneous
766 N₂O₅ Uptake During Winter: Aircraft Measurements During the 2015 WINTER Campaign and
767 Critical Evaluation of Current Parameterizations, *Journal of Geophysical Research-Atmospheres*, 123,
768 4345-4372, 10.1002/2018jd028336, 2018b.
- 769 Mentel, T. F., Sohn, M., and Wahner, A.: Nitrate effect in the heterogeneous hydrolysis of dinitrogen
770 pentoxide on aqueous aerosols, *Phys Chem Chem Phys*, 1, 5451-5457, Doi 10.1039/A905338g, 1999.
- 771 Mielke, L. H., Stutz, J., Tsai, C., Hurlock, S. C., Roberts, J. M., Veres, P. R., Froyd, K. D., Hayes, P.
772 L., Cubison, M. J., Jimenez, J. L., Washenfelder, R. A., Young, C. J., Gilman, J. B., de Gouw, J. A.,
773 Flynn, J. H., Grossberg, N., Lefter, B. L., Liu, J., Weber, R. J., and Osthoff, H. D.: Heterogeneous
774 formation of nitryl chloride and its role as a nocturnal NO_x reservoir species during CalNex-LA 2010,
775 *Journal of Geophysical Research-Atmospheres*, 118, 10638-10652, Doi 10.1002/Jgrd.50783, 2013.
- 776 Mielke, L. H., Furgeson, A., Odame-Ankrah, C. A., and Osthoff, H. D.: Ubiquity of ClNO₂ in the
777 urban boundary layer of Calgary, Alberta, Canada, *Canadian Journal of Chemistry*, 94, 414-423,
778 10.1139/cjc-2015-0426, 2015.
- 779 Mozurkewich, M., and Calvert, J. G.: Reaction Probability of N₂O₅ on Aqueous Aerosols, *Journal of*
780 *Geophysical Research-Atmospheres*, 93, 15889-15896, DOI 10.1029/JD093iD12p15889, 1988.
- 781 Osthoff, H. D., Roberts, J. M., Ravishankara, A. R., Williams, E. J., Lerner, B. M., Sommariva, R.,
782 Bates, T. S., Coffman, D., Quinn, P. K., Dibb, J. E., Stark, H., Burkholder, J. B., Talukdar, R. K.,
783 Meagher, J., Fehsenfeld, F. C., and Brown, S. S.: High levels of nitryl chloride in the polluted
784 subtropical marine boundary layer, *Nat Geosci*, 1, 324-328, Doi 10.1038/Ngeo177, 2008.
- 785 Peng, X., Wang, W., Xia, M., Chen, H., Ravishankara, A. R., Li, Q., Saiz-Lopez, A., Liu, P., Zhang, F.,
786 Zhang, C., Xue, L., Wang, X., George, C., Wang, J., Mu, Y., Chen, J., and Wang, T.: An unexpected
787 large continental source of reactive bromine and chlorine with significant impact on wintertime air
788 quality, *Natl Sci Rev*, 8, 10.1093/nsr/nwaa304, 2021.
- 789 Phillips, G. J., Tang, M. J., Thieser, J., Brickwedde, B., Schuster, G., Bohn, B., Lelieveld, J., and
790 Crowley, J. N.: Significant concentrations of nitryl chloride observed in rural continental Europe
791 associated with the influence of sea salt chloride and anthropogenic emissions, *Geophysical Research*
792 *Letters*, 39, Artn L10811
793 10.1029/2012gl051912, 2012.
- 794 Phillips, G. J., Thieser, J., Tang, M. J., Sobanski, N., Schuster, G., Fachinger, J., Drewnick, F.,



- 795 Borrmann, S., Bingemer, H., Lelieveld, J., and Crowley, J. N.: Estimating N₂O₅ uptake coefficients
796 using ambient measurements of NO₃, N₂O₅, ClNO₂ and particle-phase nitrate, *Atmospheric*
797 *Chemistry and Physics*, 16, 13231-13249, 10.5194/acp-16-13231-2016, 2016.
- 798 Riedel, T. P., Bertram, T. H., Crisp, T. A., Williams, E. J., Lerner, B. M., Vlasenko, A., Li, S. M.,
799 Gilman, J., de Gouw, J., Bon, D. M., Wagner, N. L., Brown, S. S., and Thornton, J. A.: Nitryl Chloride
800 and Molecular Chlorine in the Coastal Marine Boundary Layer, *Environmental Science & Technology*,
801 46, 10463-10470, 10.1021/es204632r, 2012.
- 802 Riedel, T. P., Wagner, N. L., Dube, W. P., Middlebrook, A. M., Young, C. J., Ozturk, F., Bahreini, R.,
803 VandenBoer, T. C., Wolfe, D. E., Williams, E. J., Roberts, J. M., Brown, S. S., and Thornton, J. A.:
804 Chlorine activation within urban or power plant plumes: Vertically resolved ClNO₂ and Cl₂
805 measurements from a tall tower in a polluted continental setting, *Journal of Geophysical Research-*
806 *Atmospheres*, 118, 8702-8715, 10.1002/jgrd.50637, 2013.
- 807 Riedel, T. P., Wolfe, G. M., Danas, K. T., Gilman, J. B., Kuster, W. C., Bon, D. M., Vlasenko, A., Li,
808 S. M., Williams, E. J., Lerner, B. M., Veres, P. R., Roberts, J. M., Holloway, J. S., Lefer, B., Brown, S.
809 S., and Thornton, J. A.: An MCM modeling study of nitryl chloride (ClNO₂) impacts on oxidation,
810 ozone production and nitrogen oxide partitioning in polluted continental outflow, *Atmospheric*
811 *Chemistry and Physics*, 14, 3789-3800, 10.5194/acp-14-3789-2014, 2014.
- 812 Roberts, J. M., Osthoff, H. D., Brown, S. S., Ravishankara, A. R., Coffman, D., Quinn, P., and Bates,
813 T.: Laboratory studies of products of N₂O₅ uptake on Cl- containing substrates, *Geophysical Research*
814 *Letters*, 36, Artn L20808
815 10.1029/2009gl040448, 2009.
- 816 Ryder, O. S., Campbell, N. R., Shalowski, M., Al-Mashat, H., Nathanson, G. M., and Bertram, T. H.:
817 Role of Organics in Regulating ClNO₂ Production at the Air-Sea Interface, *J Phys Chem A*, 119, 8519-
818 8526, 10.1021/jp5129673, 2015.
- 819 Saiz-Lopez, A., and von Glasow, R.: Reactive halogen chemistry in the troposphere, *Chem Soc Rev*,
820 41, 6448-6472, 2012.
- 821 Sarwar, G., Simon, H., Xing, J., and Mathur, R.: Importance of tropospheric ClNO₂ chemistry across
822 the Northern Hemisphere, *Geophysical Research Letters*, 41, 4050-4058, 10.1002/2014gl059962,
823 2014.
- 824 Shi, B., Wang, W., Zhou, L., Sun, Z., Fan, C., Chen, Y., Zhang, W., Qiao, Y., Qiao, Y., and Ge, M.:
825 Atmospheric oxidation of C₁₀₋₁₄ n-alkanes initiated by Cl atoms: Kinetics and mechanism,
826 *Atmospheric Environment*, 222, 10.1016/j.atmosenv.2019.117166, 2020.
- 827 Simpson, W. R., Brown, S. S., Saiz-Lopez, A., Thornton, J. A., and von Glasow, R.: Tropospheric
828 Halogen Chemistry: Sources, Cycling, and Impacts, *Chemical Reviews*, 115, 4035-4062,
829 10.1021/cr5006638, 2015.
- 830 Sommariva, R., Hollis, L. D. J., Sherwen, T., Baker, A. R., Ball, S. M., Bandy, B. J., Bell, T. G.,
831 Chowdhury, M. N., Cordell, R. L., Evans, M. J., Lee, J. D., Reed, C., Reeves, C. E., Roberts, J. M.,
832 Yang, M. X., and Monks, P. S.: Seasonal and geographical variability of nitryl chloride and its
833 precursors in Northern Europe, *Atmos Sci Lett*, 19, UNSP e844
834 10.1002/asl.844, 2018.
- 835 Staudt, S., Gord, J. R., Karimova, N. V., McDuffie, E. E., Brown, S. S., Gerber, R. B., Nathanson, G.
836 M., and Bertram, T. H.: Sulfate and Carboxylate Suppress the Formation of ClNO₂ at Atmospheric



- 837 Interfaces, *Acs Earth Space Chem*, 3, 1987-1997, 10.1021/acsearthspacechem.9b00177, 2019.
- 838 Tan, Z., Fuchs, H., Lu, K., Hofzumahaus, A., Bohn, B., Broch, S., Dong, H., Gomm, S., Haeseler, R.,
839 He, L., Holland, F., Li, X., Liu, Y., Lu, S., Rohrer, F., Shao, M., Wang, B., Wang, M., Wu, Y., Zeng, L.,
840 Zhang, Y., Wahner, A., and Zhang, Y.: Radical chemistry at a rural site (Wangdu) in the North China
841 Plain: observation and model calculations of OH, HO₂ and RO₂ radicals, *Atmospheric Chemistry and*
842 *Physics*, 17, 663-690, 10.5194/acp-17-663-2017, 2017.
- 843 Tan, Z. F., Lu, K. D., Hofzumahaus, A., Fuchs, H., Bohn, B., Holland, F., Liu, Y. H., Rohrer, F., Shao,
844 M., Sun, K., Wu, Y. S., Zeng, L. M., Zhang, Y. S., Zou, Q., Kiendler-Scharr, A., Wahner, A., and Zhang,
845 Y. H.: Experimental budgets of OH, HO₂, and RO₂ radicals and implications for ozone formation in
846 the Pearl River Delta in China 2014, *Atmospheric Chemistry and Physics*, 19, 7129-7150,
847 10.5194/acp-19-7129-2019, 2019.
- 848 Tang, M. J., Telford, P. J., Pope, F. D., Rkiouak, L., Abraham, N. L., Archibald, A. T., Braesicke, P.,
849 Pyle, J. A., McGregor, J., Watson, I. M., Cox, R. A., and Kalberer, M.: Heterogeneous reaction of
850 N₂O₅ with airborne TiO₂ particles and its implication for stratospheric particle injection, *Atmospheric*
851 *Chemistry and Physics*, 14, 6035-6048, DOI 10.5194/acp-14-6035-2014, 2014.
- 852 Thaler, R. D., Mielke, L. H., and Osthoff, H. D.: Quantification of Nitryl Chloride at Part Per Trillion
853 Mixing Ratios by Thermal Dissociation Cavity Ring-Down Spectroscopy, *Analytical Chemistry*, 83,
854 2761-2766, 10.1021/ac200055z, 2011.
- 855 Tham, Y. J., Yan, C., Xue, L. K., Zha, Q. Z., Wang, X. F., and Wang, T.: Presence of high nitryl chloride
856 in Asian coastal environment and its impact on atmospheric photochemistry, *Chinese Science Bulletin*,
857 59, 356-359, 10.1007/s11434-013-0063-y, 2014.
- 858 Tham, Y. J., Wang, Z., Li, Q. Y., Yun, H., Wang, W. H., Wang, X. F., Xue, L. K., Lu, K. D., Ma, N.,
859 Bohn, B., Li, X., Kecorius, S., Gross, J., Shao, M., Wiedensohler, A., Zhang, Y. H., and Wang, T.:
860 Significant concentrations of nitryl chloride sustained in the morning: investigations of the causes and
861 impacts on ozone production in a polluted region of northern China, *Atmospheric Chemistry and*
862 *Physics*, 16, 14959-14977, 10.5194/acp-16-14959-2016, 2016.
- 863 Tham, Y. J., Wang, Z., Li, Q. Y., Wang, W. H., Wang, X. F., Lu, K. D., Ma, N., Yan, C., Kecorius, S.,
864 Wiedensohler, A., Zhang, Y. H., and Wang, T.: Heterogeneous N₂O₅ uptake coefficient and production
865 yield of ClNO₂ in polluted northern China: roles of aerosol water content and chemical composition,
866 *Atmospheric Chemistry and Physics*, 18, 13155-13171, 10.5194/acp-18-13155-2018, 2018.
- 867 Thornton, J. A., Kercher, J. P., Riedel, T. P., Wagner, N. L., Cozic, J., Holloway, J. S., Dube, W. P.,
868 Wolfe, G. M., Quinn, P. K., Middlebrook, A. M., Alexander, B., and Brown, S. S.: A large atomic
869 chlorine source inferred from mid-continental reactive nitrogen chemistry, *Nature*, 464, 271-274,
870 10.1038/nature08905, 2010a.
- 871 Thornton, J. A., Kercher, J. P., Riedel, T. P., Wagner, N. L., Cozic, J., Holloway, J. S., Dube, W. P.,
872 Wolfe, G. M., Quinn, P. K., Middlebrook, A. M., Alexander, B., and Brown, S. S.: A large atomic
873 chlorine source inferred from mid-continental reactive nitrogen chemistry, *Nature*, 464, 271-274,
874 10.1038/nature08905, 2010b.
- 875 Veres, P. R., Neuman, J. A., Bertram, T. H., Assaf, E., Wolfe, G. M., Williamson, C. J., Weinzierl, B.,
876 Tilmes, S., Thompson, C. R., Thames, A. B., Schroder, J. C., Saiz-Lopez, A., Rollins, A. W., Roberts,
877 J. M., Price, D., Peischl, J., Nault, B. A., Moller, K. H., Miller, D. O., Meinardi, S., Li, Q., Lamarque,
878 J. F., Kupc, A., Kjaergaard, H. G., Kinnison, D., Jimenez, J. L., Jernigan, C. M., Hornbrook, R. S.,



- 879 Hills, A., Dollner, M., Day, D. A., Cuevas, C. A., Campuzano-Jost, P., Burkholder, J., Bui, T. P., Brune,
880 W. H., Brown, S. S., Brock, C. A., Bourgeois, I., Blake, D. R., Apel, E. C., and Ryerson, T. B.: Global
881 airborne sampling reveals a previously unobserved dimethyl sulfide oxidation mechanism in the
882 marine atmosphere, *Proc Natl Acad Sci U S A*, 117, 4505-4510, 10.1073/pnas.1919344117, 2020.
- 883 Wagner, N. L., Riedel, T. P., Roberts, J. M., Thornton, J. A., Angevine, W. M., Williams, E. J., Lerner,
884 B. M., Vlasenko, A., Li, S. M., Dube, W. P., Coffman, D. J., Bon, D. M., de Gouw, J. A., Kuster, W.
885 C., Gilman, J. B., and Brown, S. S.: The sea breeze/land breeze circulation in Los Angeles and its
886 influence on nitryl chloride production in this region, *Journal of Geophysical Research-Atmospheres*,
887 117, ArtD00v24
888 10.1029/2012jd017810, 2012.
- 889 Wahner, A., Mentel, T. F., Sohn, M., and Stier, J.: Heterogeneous reaction of N₂O₅ on sodium nitrate
890 aerosol, *Journal of Geophysical Research-Atmospheres*, 103, 31103-31112, Doi
891 10.1029/1998jd100022, 1998.
- 892 Wang, H., Lu, K., Chen, X., Zhu, Q., Chen, Q., Guo, S., Jiang, M., Li, X., Shang, D., Tan, Z., Wu, Y.,
893 Wu, Z., Zou, Q., Zheng, Y., Zeng, L., Zhu, T., Hu, M., and Zhang, Y.: High N₂O₅ Concentrations
894 Observed in Urban Beijing: Implications of a Large Nitrate Formation Pathway, *Environmental
895 Science & Technology Letters*, 4, 416-420, 10.1021/acs.estlett.7b00341, 2017a.
- 896 Wang, H., Lu, K., Tan, Z., Sun, K., Li, X., Hu, M., Shao, M., Zeng, L., Zhu, T., and Zhang, Y.: Model
897 simulation of NO₃, N₂O₅ and ClNO₂ at a rural site in Beijing during CAREBeijing-2006,
898 *Atmospheric Research*, 196, 97-107, 10.1016/j.atmosres.2017.06.013, 2017b.
- 899 Wang, H., Lu, K., Guo, S., Wu, Z., Shang, D., Tan, Z., Wang, Y., Le Breton, M., Lou, S., Tang, M.,
900 Wu, Y., Zhu, W., Zheng, J., Zeng, L., Hallquist, M., Hu, M., and Zhang, Y.: Efficient N₂O₅ uptake and
901 NO₃ oxidation in the outflow of urban Beijing, *Atmospheric Chemistry and Physics*, 18, 9705-9721,
902 10.5194/acp-18-9705-2018, 2018.
- 903 Wang, H., and Lu, K.: Monitoring Ambient Nitrate Radical by Open-Path Cavity-Enhanced Absorption
904 Spectroscopy, *Analytical Chemistry*, 91, 10687-10693, 10.1021/acs.analchem.9b01971, 2019.
- 905 Wang, H., Chen, X., Lu, K., Tan, Z., Ma, X., Wu, Z., Li, X., Liu, Y., Shang, D., Wu, Y., Zeng, L., Hu,
906 M., Schmitt, S., Kiendler-Scharr, A., Wahner, A., and Zhang, Y.: Wintertime N₂O₅ uptake coefficients
907 over the North China Plain, *Science Bulletin*, 65, 765-774, 10.1016/j.scib.2020.02.006, 2020a.
- 908 Wang, H., Peng, C., Wang, X., Lou, S., Lu, K., Gan, G., Jia, X., Chen, X., Chen, J., Wang, H., Fan, S.,
909 Wang, X., and Tang, M.: N₂O₅ uptake onto saline mineral dust: a potential
910 missing source of tropospheric ClNO₂ in inland China, *Atmospheric Chemistry and
911 Physics*, 22, 1845-1859, 10.5194/acp-22-1845-2022, 2022a.
- 912 Wang, K., Wang, W., Fan, C., Li, J., Lei, T., Zhang, W., Shi, B., Chen, Y., Liu, M., Lian, C., Wang, Z.,
913 and Ge, M.: Reactions of C₁₂-C₁₄ n-Alkylcyclohexanes with Cl Atoms: Kinetics and Secondary
914 Organic Aerosol Formation, *Environmental Science & Technology*, 56, 4859-4870,
915 10.1021/acs.est.1c08958, 2022b.
- 916 Wang, T., Tham, Y. J., Xue, L. K., Li, Q. Y., Zha, Q. Z., Wang, Z., Poon, S. C. N., Dube, W. P., Blake,
917 D. R., Louie, P. K. K., Luk, C. W. Y., Tsui, W., and Brown, S. S.: Observations of nitryl chloride and
918 modeling its source and effect on ozone in the planetary boundary layer of southern China, *Journal of
919 Geophysical Research-Atmospheres*, 121, 2476-2489, 10.1002/2015jd024556, 2016.
- 920 Wang, T., Dai, J. N., Lam, K. S., Poon, C. N., and Brasseur, G. P.: Twenty-Five Years of Lower



- 921 Tropospheric Ozone Observations in Tropical East Asia: The Influence of Emissions and Weather
922 Patterns, *Geophysical Research Letters*, 46, 11463-11470, 10.1029/2019gl084459, 2019a.
- 923 Wang, W., Yuan, B., Peng, Y., Su, H., Cheng, Y., Yang, S., Wu, C., Qi, J., Bao, F., Huangfu, Y., Wang,
924 C., Ye, C., Wang, Z., Wang, B., Wang, X., Song, W., Hu, W., Cheng, P., Zhu, M., Zheng, J., and Shao,
925 M.: Direct observations indicate photodegradable oxygenated volatile organic compounds (OVOCs)
926 as larger contributors to radicals and ozone production in the atmosphere, *Atmospheric Chemistry and*
927 *Physics*, 22, 4117-4128, 10.5194/acp-22-4117-2022, 2022c.
- 928 Wang, X., Jacob, D. J., Eastham, S. D., Sulprizio, M. P., Zhu, L., Chen, Q., Alexander, B., Sherwen,
929 T., Evans, M. J., Lee, B. H., Haskins, J. D., Lopez-Hilfiker, F. D., Thornton, J. A., Huey, G. L., and
930 Liao, H.: The role of chlorine in global tropospheric chemistry, *Atmospheric Chemistry and Physics*,
931 19, 3981-4003, 10.5194/acp-19-3981-2019, 2019b.
- 932 Wang, X., Jacob, D. J., Eastham, S. D., Sulprizio, M. P., Zhu, L., Chen, Q. J., Alexander, B., Sherwen,
933 T., Evans, M. J., Lee, B. H., Haskins, J. D., Lopez-Hilfiker, F. D., Thornton, J. A., Huey, G. L., and
934 Liao, H.: The role of chlorine in global tropospheric chemistry, *Atmospheric Chemistry and Physics*,
935 19, 3981-4003, 10.5194/acp-19-3981-2019, 2019c.
- 936 Wang, X. F., Wang, H., Xue, L. K., Wang, T., Wang, L. W., Gu, R. R., Wang, W. H., Tham, Y. J., Wang,
937 Z., Yang, L. X., Chen, J. M., and Wang, W. X.: Observations of N₂O₅ and ClNO₂ at a polluted urban
938 surface site in North China: High N₂O₅ uptake coefficients and low ClNO₂ product yields,
939 *Atmospheric Environment*, 156, 125-134, 10.1016/j.atmosenv.2017.02.035, 2017c.
- 940 Wang, Z., Wang, W. H., Tham, Y. J., Li, Q. Y., Wang, H., Wen, L., Wang, X. F., and Wang, T.: Fast
941 heterogeneous N₂O₅ uptake and ClNO₂ production in power plant and industrial plumes observed in
942 the nocturnal residual layer over the North China Plain, *Atmospheric Chemistry and Physics*, 17,
943 12361-12378, 10.5194/acp-17-12361-2017, 2017d.
- 944 Wang, Z., Yuan, B., Ye, C., Roberts, J., Wisthaler, A., Lin, Y., Li, T., Wu, C., Peng, Y., Wang, C., Wang,
945 S., Yang, S., Wang, B., Qi, J., Wang, C., Song, W., Hu, W., Wang, X., Xu, W., Ma, N., Kuang, Y., Tao,
946 J., Zhang, Z., Su, H., Cheng, Y., Wang, X., and Shao, M.: High Concentrations of Atmospheric
947 Isocyanic Acid (HNCO) Produced from Secondary Sources in China, *Environmental Science &*
948 *Technology*, 54, 11818-11826, 10.1021/acs.est.0c02843, 2020b.
- 949 Wu, C., Wang, C., Wang, S., Wang, W., Yuan, B., Qi, J., Wang, B., Wang, H., Wang, C., Song, W.,
950 Wang, X., Hu, W., Lou, S., Ye, C., Peng, Y., Wang, Z., Huangfu, Y., Xie, Y., Zhu, M., Zheng, J., Wang,
951 X., Jiang, B., Zhang, Z., and Shao, M.: Measurement report: Important contributions of oxygenated
952 compounds to emissions and chemistry of volatile organic compounds in urban air, *Atmos. Chem.*
953 *Phys.*, 20, 14769-14785, 10.5194/acp-20-14769-2020, 2020.
- 954 Xia, M., Peng, X., Wang, W., Yu, C., Sun, P., Li, Y., Liu, Y., Xu, Z., Wang, Z., Xu, Z., Nie, W., Ding,
955 A., and Wang, T.: Significant production of ClNO₂ and possible source of
956 Cl₂ from N₂O₅ and O₃ uptake at a
957 suburban site in eastern China, *Atmospheric Chemistry and Physics*, 20, 6147-6158, 10.5194/acp-20-
958 6147-2020, 2020.
- 959 Xia, M., Peng, X., Wang, W. H., Yu, C. A., Wang, Z., Tham, Y. J., Chen, J. M., Chen, H., Mu, Y. J.,
960 Zhang, C. L., Liu, P. F., Xue, L. K., Wang, X. F., Gao, J., Li, H., and Wang, T.: Winter ClNO₂ formation
961 in the region of fresh anthropogenic emissions: seasonal variability and insights into daytime peaks in
962 northern China, *Atmospheric Chemistry and Physics*, 21, 15985-16000, 10.5194/acp-21-15985-2021,



963 2021.

964 Xue, L. K., Saunders, S. M., Wang, T., Gao, R., Wang, X. F., Zhang, Q. Z., and Wang, W. X.:

965 Development of a chlorine chemistry module for the Master Chemical Mechanism, *Geoscientific*

966 *Model Development*, 8, 3151-3162, 10.5194/gmd-8-3151-2015, 2015.

967 Yang, S., Yuan, B., Peng, Y., Huang, S., Chen, W., Hu, W., Pei, C., Zhou, J., Parrish, D. D., Wang, W.,

968 He, X., Cheng, C., Li, X.-B., Yang, X., Song, Y., Wang, H., Qi, J., Wang, B., Wang, C., Wang, C.,

969 Wang, Z., Li, T., Zheng, E., Wang, S., Wu, C., Cai, M., Ye, C., Song, W., Cheng, P., Chen, D., Wang,

970 X., Zhang, Z., Wang, X., Zheng, J., and Shao, M.: The formation and mitigation of nitrate pollution:

971 comparison between urban and suburban environments, *Atmospheric Chemistry and Physics*, 22,

972 4539-4556, 10.5194/acp-22-4539-2022, 2022a.

973 Yang, X., Wang, T., Xia, M., Gao, X. M., Li, Q. Y., Zhang, N. W., Gao, Y., Lee, S. C., Wang, X. F.,

974 Xue, L. K., Yang, L. X., and Wang, W. X.: Abundance and origin of fine particulate chloride in

975 continental China, *Science of the Total Environment*, 624, 1041-1051,

976 10.1016/j.scitotenv.2017.12.205, 2018.

977 Yang, X., Wang, Q., Ma, N., Hu, W., Gao, Y., Huang, Z., Zheng, J., Yuan, B., Yang, N., Tao, J., Hong,

978 J., Cheng, Y., and Su, H.: The impact of chlorine chemistry combined with heterogeneous

979 N_2O_5 reactions on air quality in China, *Atmospheric Chemistry and Physics*, 22, 3743-3762, 10.5194/acp-22-3743-2022, 2022b.

980 Ye, C., Yuan, B., Lin, Y., Wang, Z., Hu, W., Li, T., Chen, W., Wu, C., Wang, C., Huang, S., Qi, J., Wang,

981 B., Wang, C., Song, W., Wang, X., Zheng, E., Krechmer, J. E., Ye, P., Zhang, Z., Wang, X., Worsnop,

982 D. R., and Shao, M.: Chemical characterization of oxygenated organic compounds in the gas phase

983 and particle phase using iodide CIMS with FIGAERO in urban air, *Atmos. Chem. Phys.*, 21, 8455-

984 8478, 10.5194/acp-21-8455-2021, 2021.

985

986 Young, C. J., Washenfelder, R. A., Roberts, J. M., Mielke, L. H., Osthoff, H. D., Tsai, C., Pikelnaya,

987 O., Stutz, J., Veres, P. R., Cochran, A. K., VandenBoer, T. C., Flynn, J., Grossberg, N., Haman, C. L.,

988 Lefer, B., Stark, H., Graus, M., de Gouw, J., Gilman, J. B., Kuster, W. C., and Brown, S. S.: Vertically

989 Resolved Measurements of Nighttime Radical Reservoirs; in Los Angeles and Their Contribution to

990 the Urban Radical Budget, *Environmental Science & Technology*, 46, 10965-10973,

991 10.1021/es302206a, 2012.

992 Yu, C., Wang, Z., Xia, M., Fu, X., Wang, W., Tham, Y. J., Chen, T., Zheng, P., Li, H., Shan, Y., Wang,

993 X., Xue, L., Zhou, Y., Yue, D., Ou, Y., Gao, J., Lu, K., Brown, S. S., Zhang, Y., and Wang, T.:

994 Heterogeneous N_2O_5 reactions on atmospheric aerosols at four Chinese sites: improving model

995 representation of uptake parameters, *Atmos. Chem. Phys.*, 20, 4367-4378, 10.5194/acp-20-4367-2020,

996 2020.

997 Yun, H., Wang, T., Wang, W. H., Tham, Y. J., Li, Q. Y., Wang, Z., and Poon, S. C. N.: Nighttime NO_x

998 loss and ClNO_2 formation in the residual layer of a polluted region: Insights from field measurements

999 and an iterative box model, *Science of the Total Environment*, 622, 727-734,

1000 10.1016/j.scitotenv.2017.11.352, 2018a.

1001 Yun, H., Wang, W. H., Wang, T., Xia, M., Yu, C., Wang, Z., Poon, S. C. N., Yue, D. L., and Zhou, Y.:

1002 Nitrate formation from heterogeneous uptake of dinitrogen pentoxide during a severe winter haze in

1003 southern China, *Atmospheric Chemistry and Physics*, 18, 17515-17527, 10.5194/acp-18-17515-2018,

1004 2018b.



1005 Zhou, W., Zhao, J., Ouyang, B., Mehra, A., Xu, W. Q., Wang, Y. Y., Bannan, T. J., Worrall, S. D.,
1006 Priestley, M., Bacak, A., Chen, Q., Xie, C. H., Wang, Q. Q., Wang, J. F., Du, W., Zhang, Y. J., Ge, X.
1007 L., Ye, P. L., Lee, J. D., Fu, P. Q., Wang, Z. F., Worsnop, D., Jones, R., Percival, C. J., Coe, H., and
1008 Sun, Y. L.: Production of N₂O₅ and ClNO₂ in summer in urban Beijing, China, *Atmospheric*
1009 *Chemistry and Physics*, 18, 11581-11597, [10.5194/acp-18-11581-2018](https://doi.org/10.5194/acp-18-11581-2018), 2018.
1010 Zong, T., Wang, H., Wu, Z., Lu, K., Wang, Y., Zhu, Y., Shang, D., Fang, X., Huang, X., He, L., Ma, N.,
1011 GroSs, J., Huang, S., Guo, S., Zeng, L., Herrmann, H., Wiedensohler, A., Zhang, Y., and Hu, M.:
1012 Particle hygroscopicity inhomogeneity and its impact on reactive uptake, *The Science of the total*
1013 *environment*, 151364-151364, [10.1016/j.scitotenv.2021.151364](https://doi.org/10.1016/j.scitotenv.2021.151364), 2021.
1014